Supporting Information for

A Switchable Dimeric Yttrium Complex and Its Three Catalytic States in Ring Opening Polymerization

*Shijie Deng and Paula L. Diaconescu**

Department of Chemistry and Biochemistry, University of California, Los Angeles, 607 Charles E. Young Drive East, Los Angeles, CA 90095

Table of Contents

NMR spectra

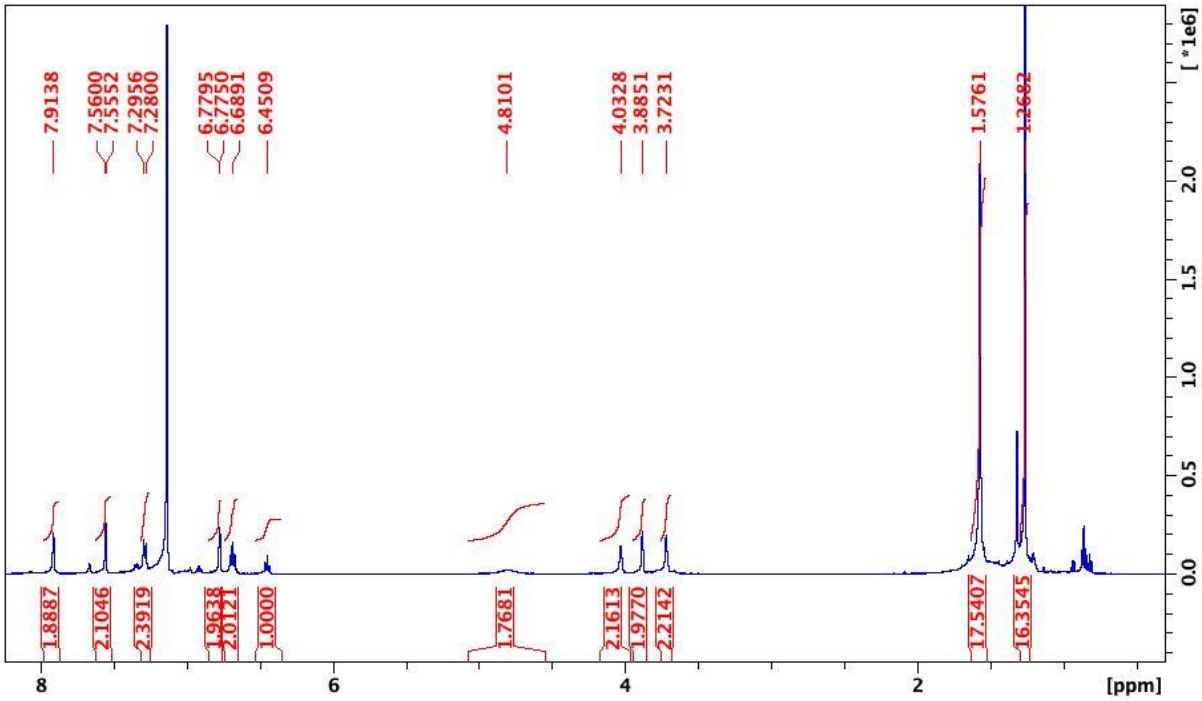

Figure S1. ^{1}H NMR (C_6D_6, 500 MHz, 298 K) spectrum of [(salfen)Y(OPh)]$_2$ δ (ppm): 7.91 (s, 2H, N=C*H*), 7.56 (d, 2H, Ar*H*), 7.29 (d, 2H, Ar*H*), 6.78 (d, 2H, Ar*H*), 6.69 (t, 2H, Ar*H*), 6.45 (t, 1H, Ar*H*), 4.81 (s, 2H, fc-*H*), 3.72-4.03 (s, s and s, 6H, fc-*H*), 1.58 (s, 18H, C(C*H*$_3$)$_3$), 1.27 (s, 18H, C(C*H*$_3$)$_3$).

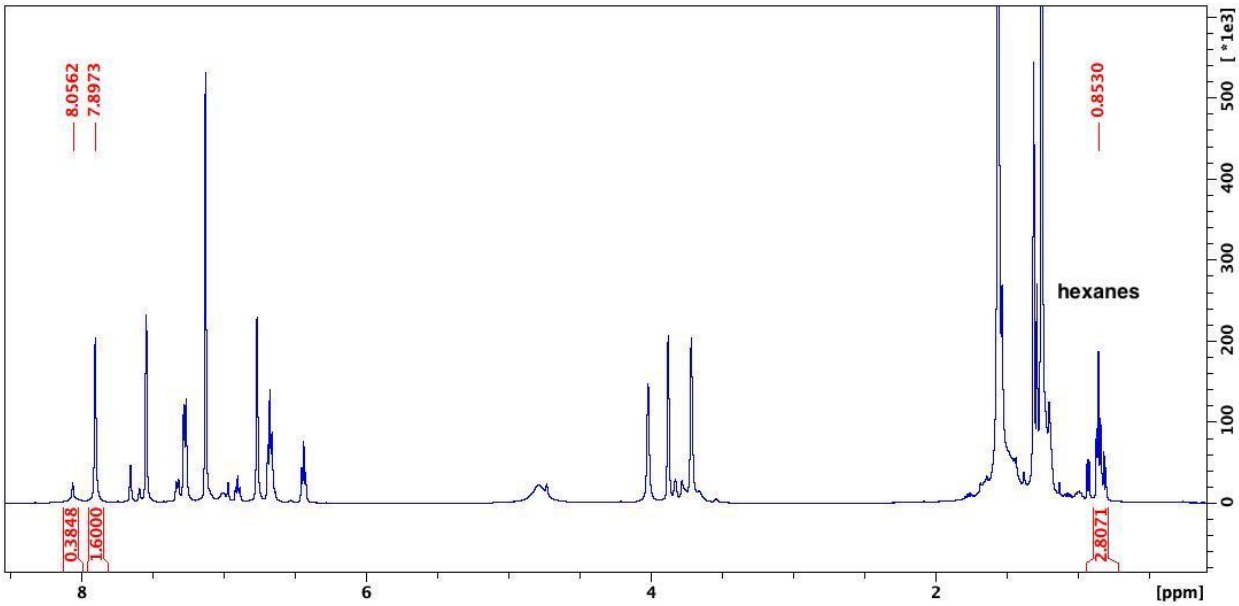

Figure S2. ^{1}H NMR (C_6D_6, 500 MHz, 298 K) spectrum of [(salfen)Y(OPh)]$_2$. The peaks at 8.05 ppm and 7.90 ppm integrate together to 2 H atoms. The peak at 0.85 ppm, which represents hexanes remaining in the sample, integrates as 2.80 H. The integration indicates that the formula of the sample is [(salfen)Y(OPh)]$_2$•(C_6H_{14})$_{0.2}$.

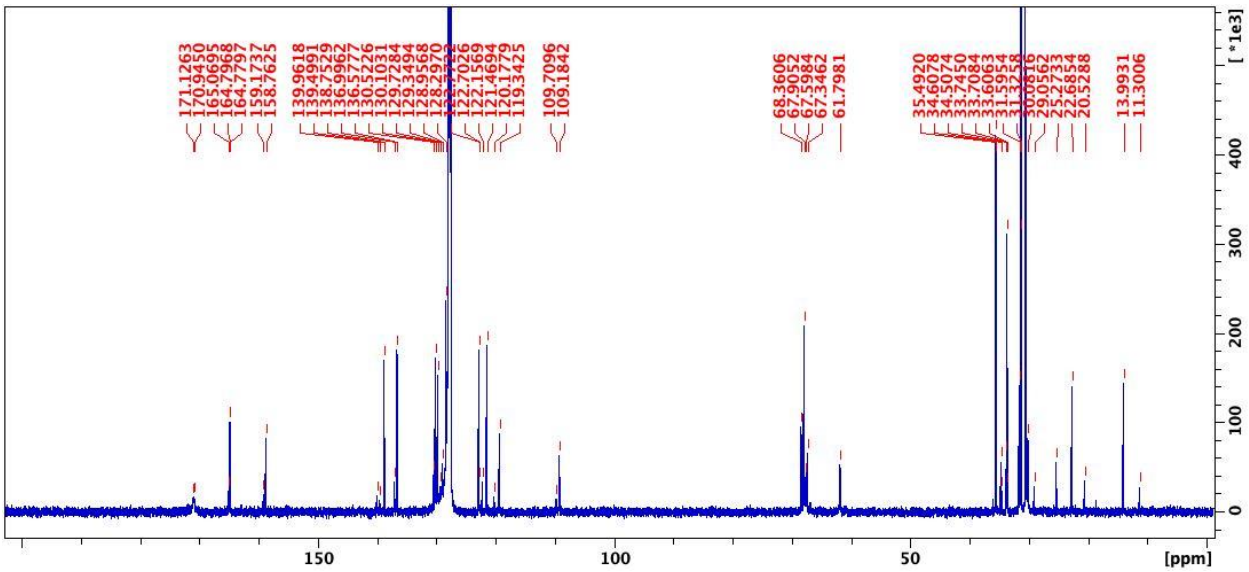

Figure S3. $^{13}C\{^1H\}$ NMR (C_6D_6, 125 MHz, 298 K) spectrum of $[(salfen)Y(OPh)]_2$ δ (ppm): 164.8 (N=*C*), 158.8 (m-OC_6H_2), 138.8 (m-OC_6H_2), 136.6 (m-OC_6H_2), 130.1 (m-OC_6H_5), 129.7 (m-OC_6H_5), 128.3 (m-OC_6H_2), 122.7 (m-OC_6H_2), 121.4(m-OC_6H_2), 119.3 (m-OC_6H_5), 109.2 (m-OC_6H_5), 61.8-68.3(C_5H_4), 34.5 ($C(CH_3)_3$), 33.6 ($C(CH_3)_3$), 31.3 ($C(CH_3)_3$), 30.5 ($C(CH_3)_3$).

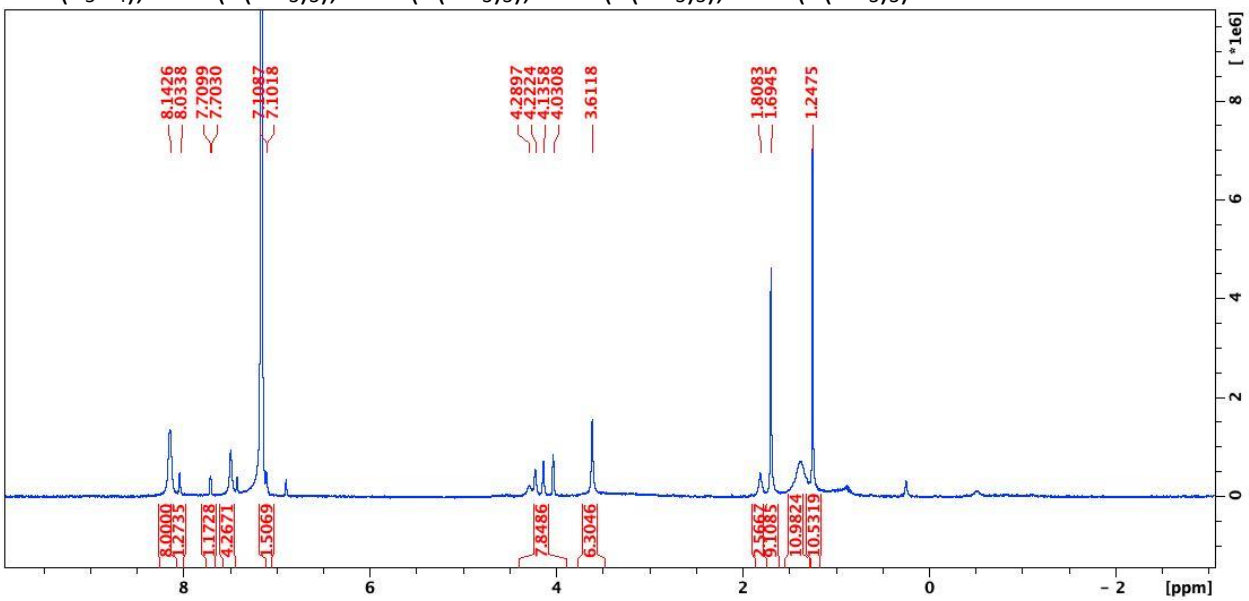

Figure S4. ^1H NMR (C_6D_6, 300 MHz, 298 K) spectrum of $[(salfen)Y(OPh)]_2[BAr^F]$ δ (ppm): 8.14 (s, 8H, BAr^F, *o*-Ar*H*), 8.03 (d, 2H, Ar*H*), 7.70 (d, 2H, Ar*H*), 7.49 (s, 4H, BAr^F, *p*-Ar*H*), 4.03-4.29 (m, 8H, Cp-*H*), 3.61 (s, 9H, $C(CH_3)_3$), 1.69 (s, 9H, $C(CH_3)_3$), 1.34 (br, 9H, $C(CH_3)_3$), 1.24 (s, 9H, $C(CH_3)_3$). Other ^1H NMR peaks were not observed due to the paramagnetic nature of this compound.

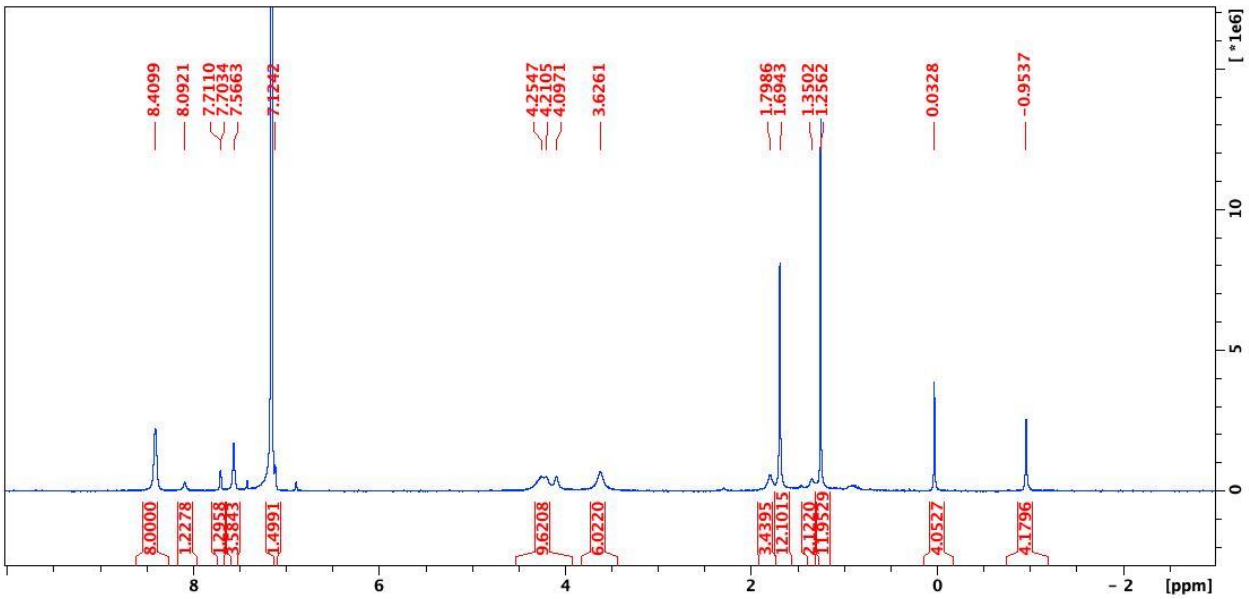

Figure S5. ^{1}H NMR (C_6D_6, 300 MHz, 298 K) spectrum of $[(salfen)Y(OPh)]_2[BAr^F]_2$ δ (ppm): 8.41 (s, 8H, BAr^F, *o*-Ar*H*), 8.09 (d, 2H, Ar*H*), 7.71 (d, 2H, Ar*H*), 7.56 (s, 4H, BAr^F, *p*-Ar*H*), 4.09-4.25 (m, 8H, Ar*H*), 3.63 (br, 9H, $C(CH_3)_3$), 1.69 (s, 9H, $C(CH_3)_3$), 1.25 (s, 9H, $C(CH_3)_3$), 0.03 (s, 24H, Cp-*H*), -0.95 (s, 4H, Cp-*H*). Other ^{1}H NMR peaks were not observed due to the paramagnetic nature of this compound.

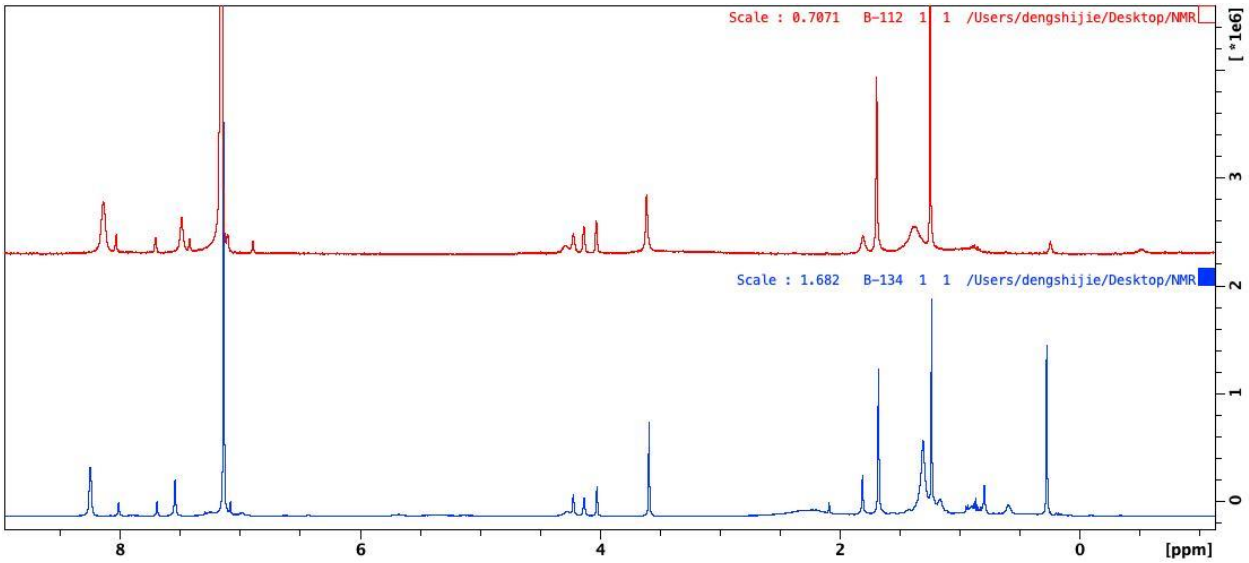

Figure S6. ^{1}H NMR (C_6D_6, 300 MHz, 298 K) spectrum of $[(salfen)Y(OPh)]_2[BAr^F]$ (top) and $[(salfen)Y(OPh)]_2$ +1 equivalent of $[(salfen)Y(OPh)]_2[BAr^F]_2$ (bottom).

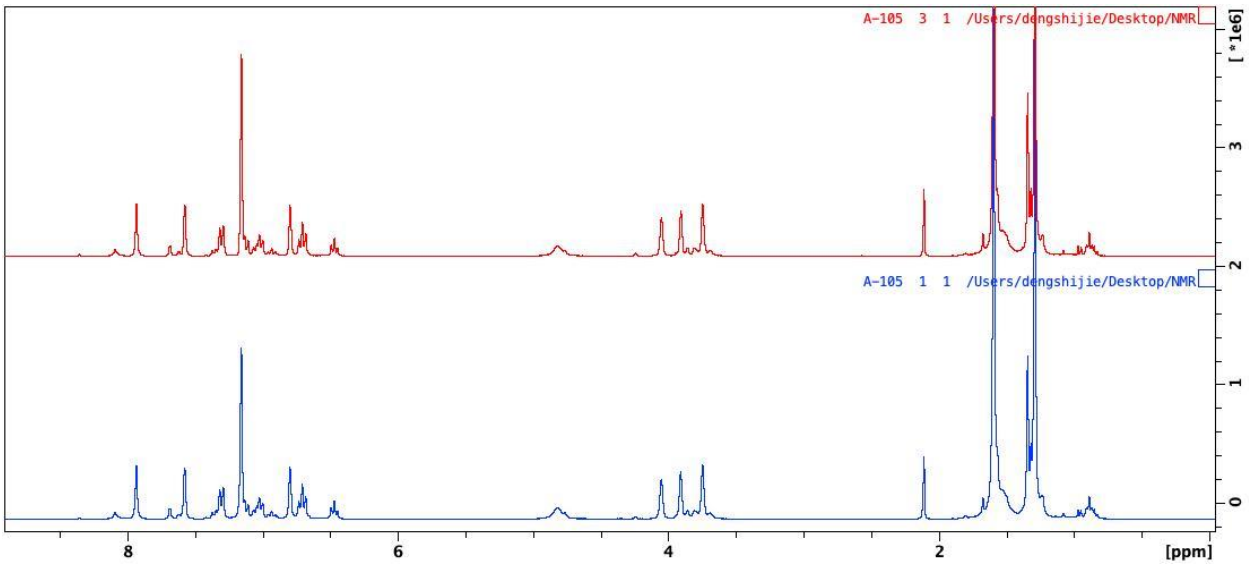

Figure S7. Thermal decomposition study (C_6D_6, 300 MHz, 298 K) of $[(salfen)Y(OPh)]_2$. $[(salfen)Y(OPh)]_2$ before heating (bottom) and after heating at 80°C for 24 h (top).

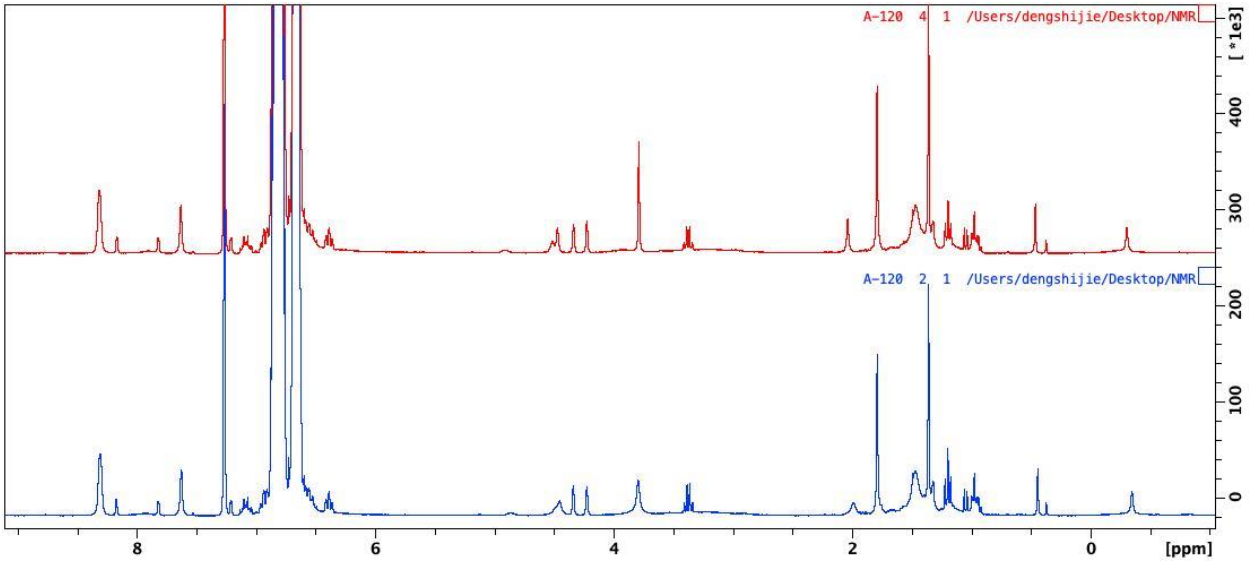

Figure S8. Thermal decomposition study (C_6D_6, 300 MHz, 298 K) of $[(salfen)Y(OPh)]_2[BAr^F]$. $[(salfen)Y(OPh)]_2[BAr^F]$ generated *in situ* before heating (bottom) and after heating at 80°C for 24 h (top).

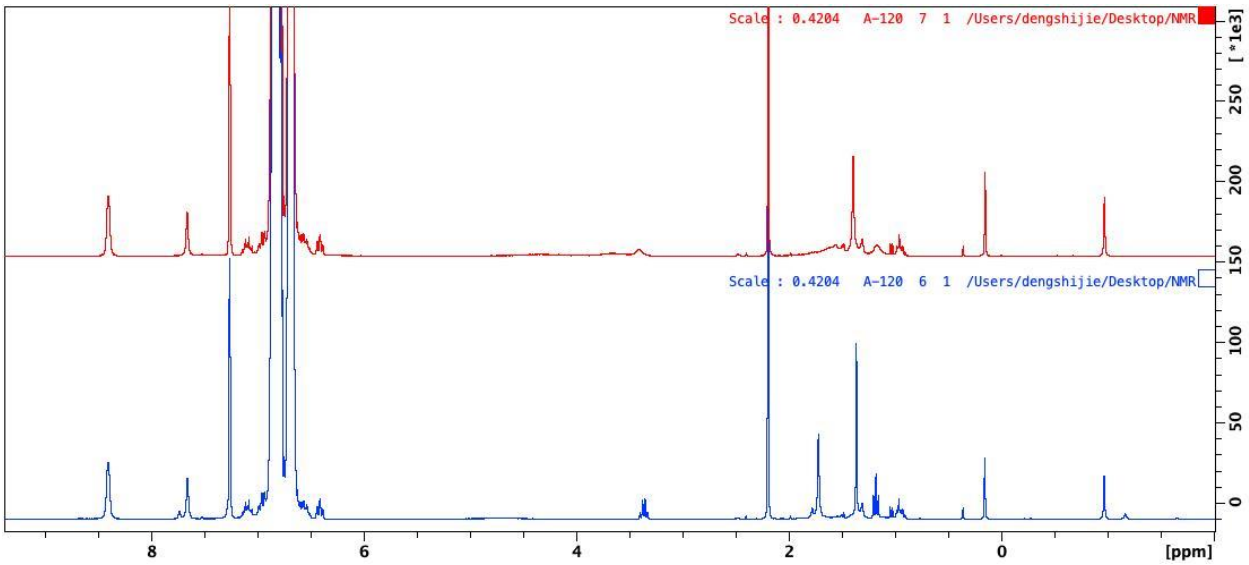

Figure S9. Thermal decomposition study (C_6D_6, 300 MHz, 298 K) of $[(salfen)Y(OPh)]_2[BAr^F]_2$. $[(salfen)Y(OPh)]_2[BAr^F]_2$ generated *in situ* before heating (bottom) and after heating at 80°C for 24 h (top).

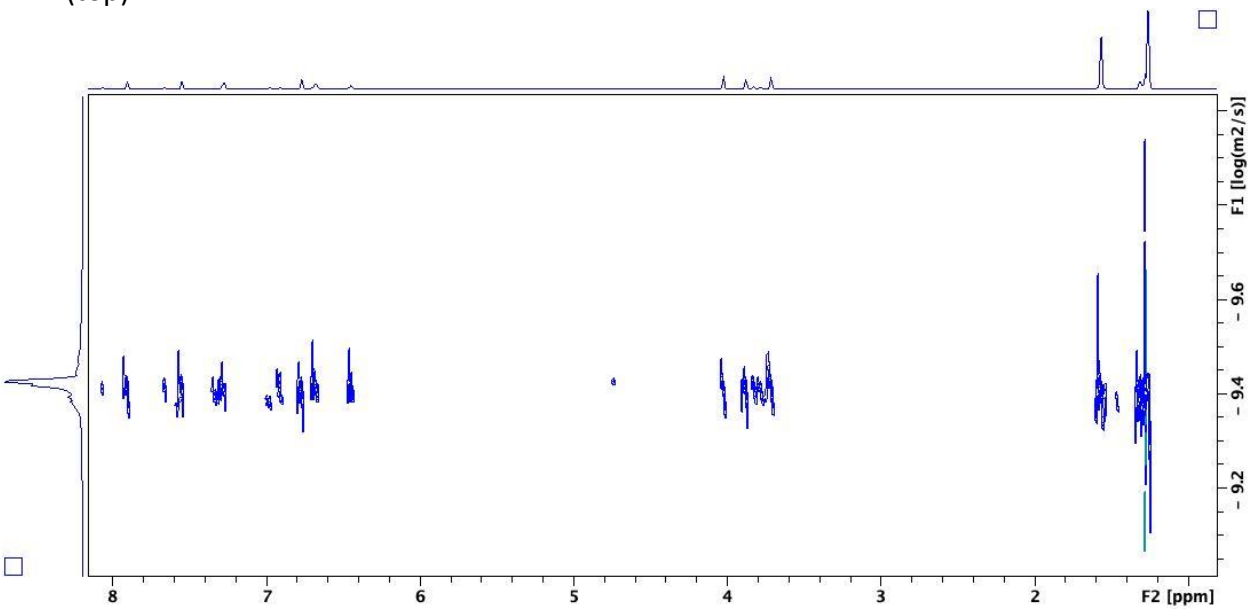

Figure S10. DOSY (C_6D_6, 500 MHz, 298 K) of $[(salfen)Y(OPh)]_2$.

Radius in benzene, r_H: Stoke-Einstein equation $D = (kT)/(6\pi\eta r_H)$ was used to calculated hydrodynamic radius in solution, D was obtained from DOSY NMR spectrum.

Radius in solid state, $r_{X\text{-}ray}$: The molecular volume was obtained from Olex2.[1] The molecule was assumed to be a sphere and the solid-state radius was calculated using the sphere volume equation.

Reference: 1. O. V. Dolomanov, L. J. Bourhis, R. J. Gildea, J. A. K. Howard and H. Puschmann, *J. Appl. Crystallogr.*, 2009, **42**, 339-341.

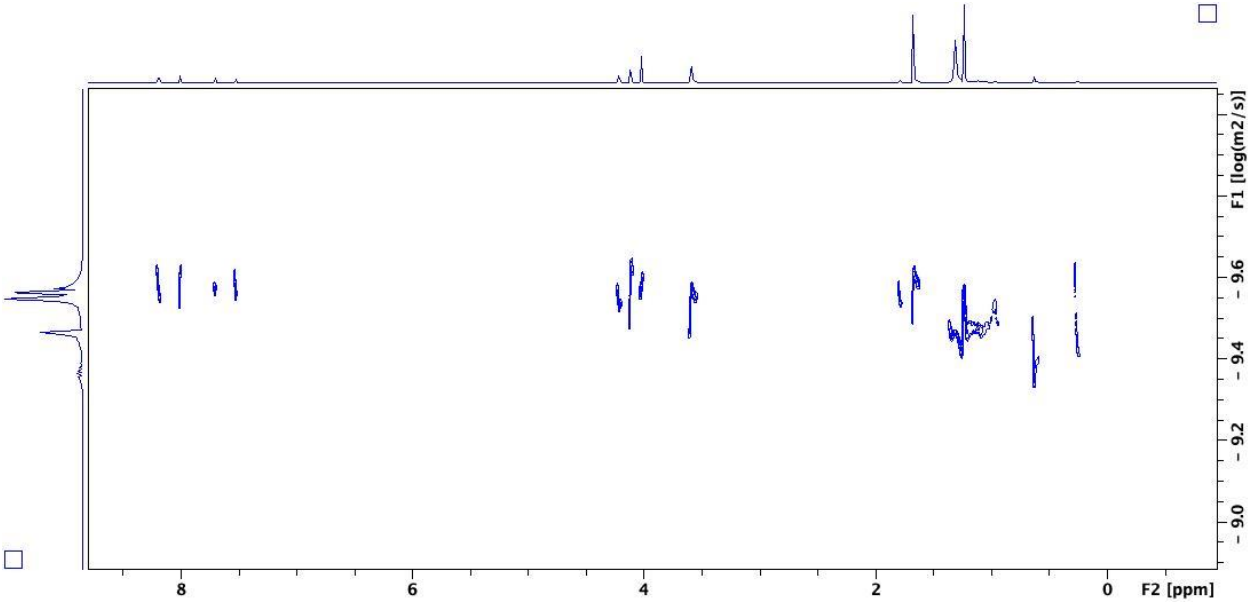

Figure S11. DOSY (C_6D_6, 500 MHz, 298 K) of $[(salfen)Y(OPh)]_2[BAr^F]$.

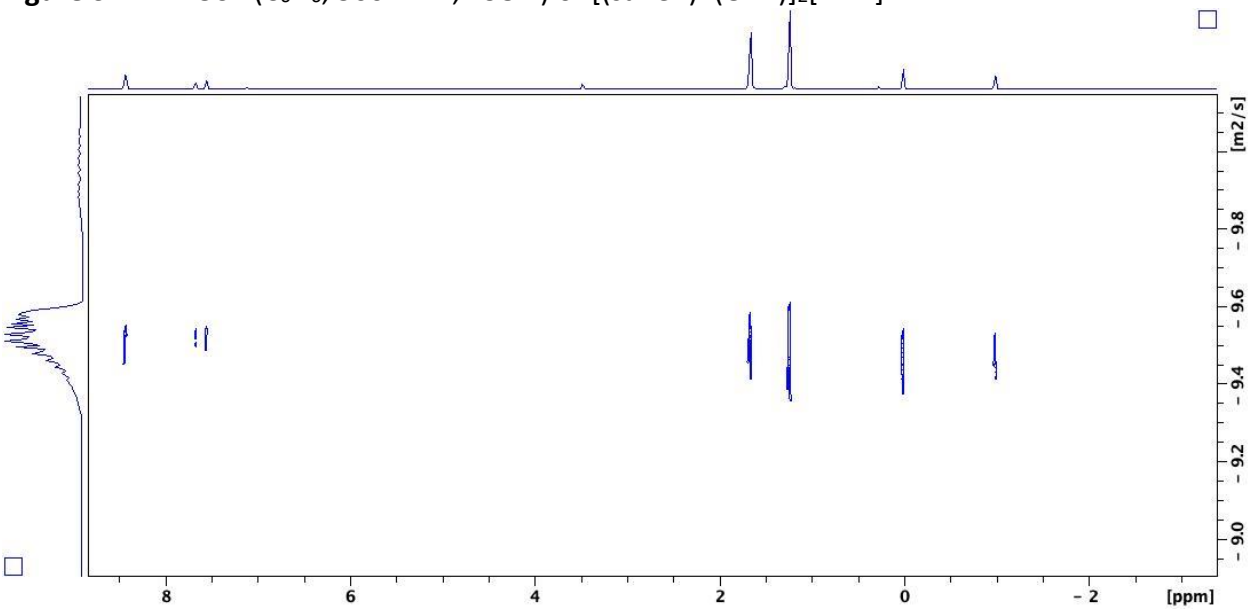

Figure S12. DOSY (C_6D_6, 500 MHz, 298 K) of $[(salfen)Y(OPh)]_2[BAr^F]_2$.

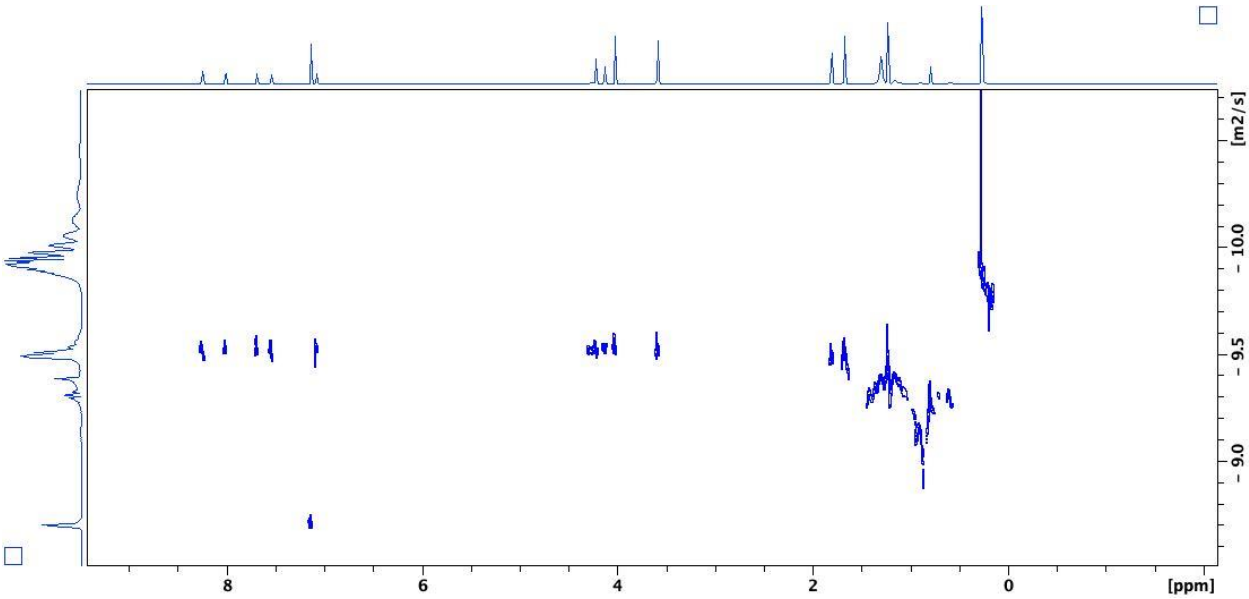

Figure S13. DOSY (C_6D_6, 500 MHz, 298 K) of $[(salfen)Y(OPh)]_2$ + 1 equivalent of $[(salfen)Y(OPh)]_2[BAr^F]_2$.

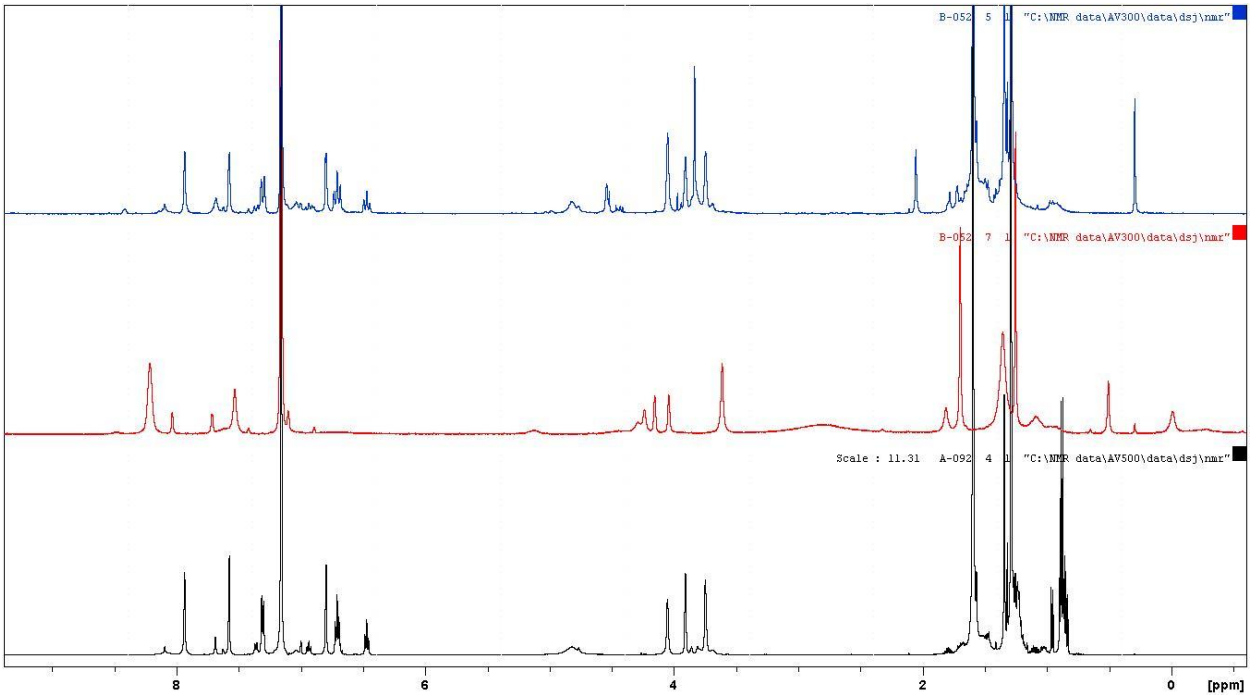

Figure S14. ^1H NMR (C_6D_6, 300 MHz, 298 K) spectrum of $[(salfen)Y(OPh)]_2$ (bottom), $[(salfen)Y(OPh)]_2[BAr^F]$ generated in situ (middle), and $[(salfen)Y(OPh)]_2$ generated from $[(salfen)Y(OPh)]_2[BAr^F]$ (top). All the peaks in the top spectrum match those in the bottom spectrum. The extra peaks in the bottom spectrum belong to ^{Ac}Fc and $CoCp_2[BAr^F]$.

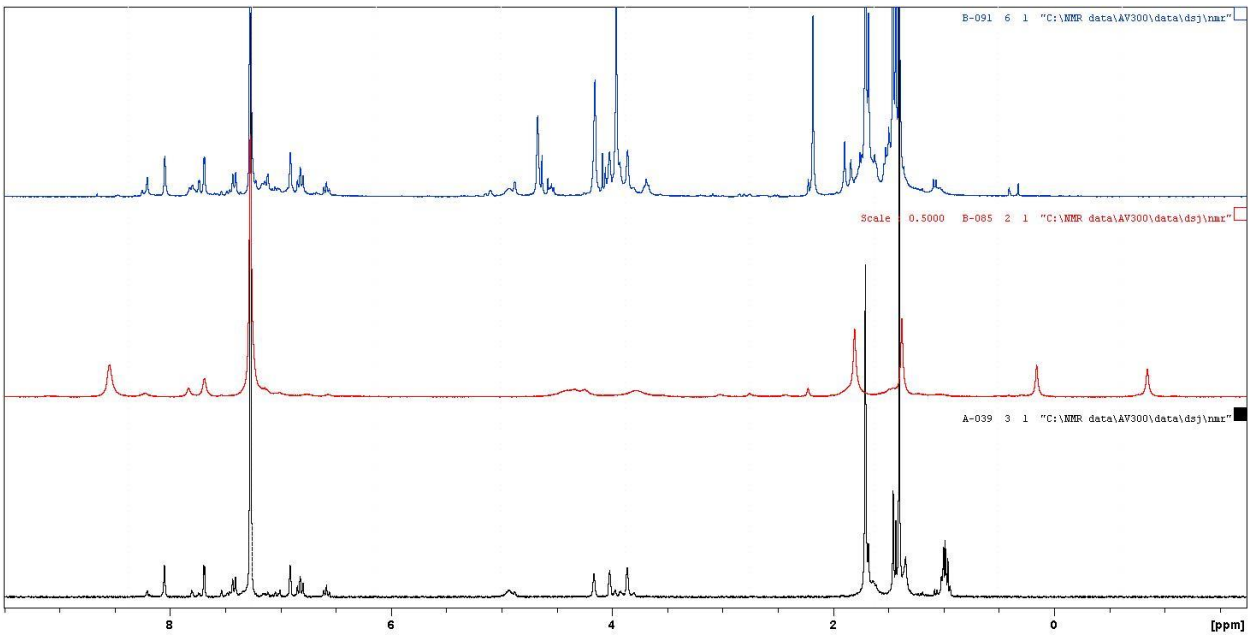

Figure S15. ^{1}H NMR (C_6D_6, 300 MHz, 298 K) spectrum of $[(salfen)Y(OPh)]_2$ (bottom), $[(salfen)Y(OPh)]_2[BAr^F]_2$ generated in situ (middle), and $[(salfen)Y(OPh)]_2$ generated from $[(salfen)Y(OPh)]_2[BAr^F]_2$ (top). All the peaks in the top spectrum match those in the bottom spectrum. The extra peaks in the bottom spectrum belong to AcFc and $CoCp_2[BAr^F]$.

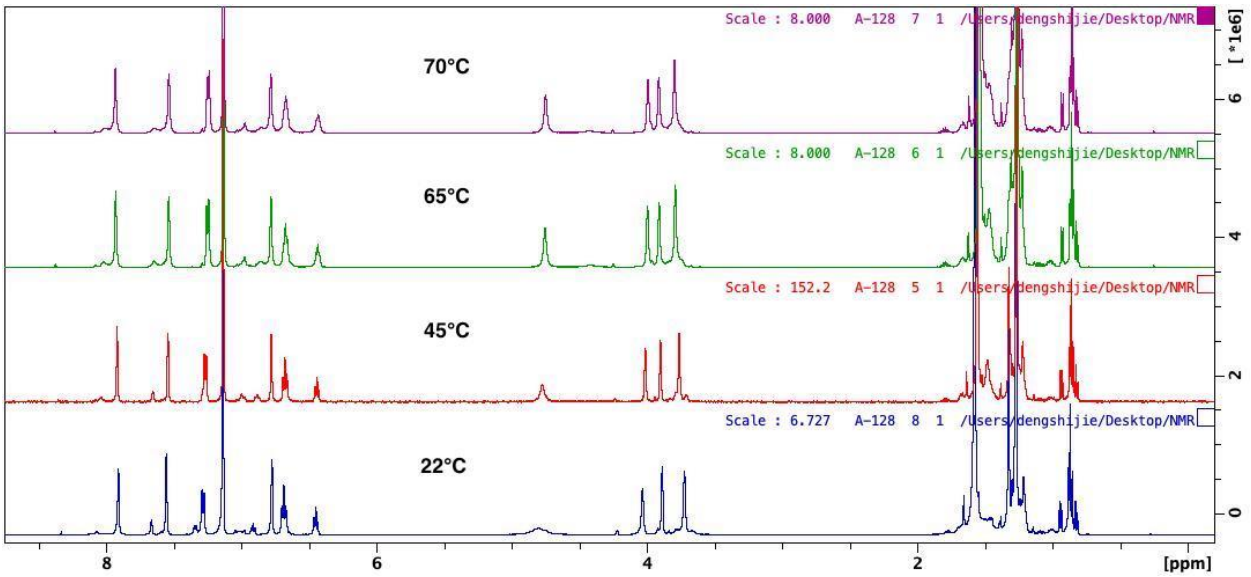

Figure S16. Variable temperature ^{1}H NMR (C_6D_6, 500 MHz) study of $[(salfen)Y(OPh)]_2$.

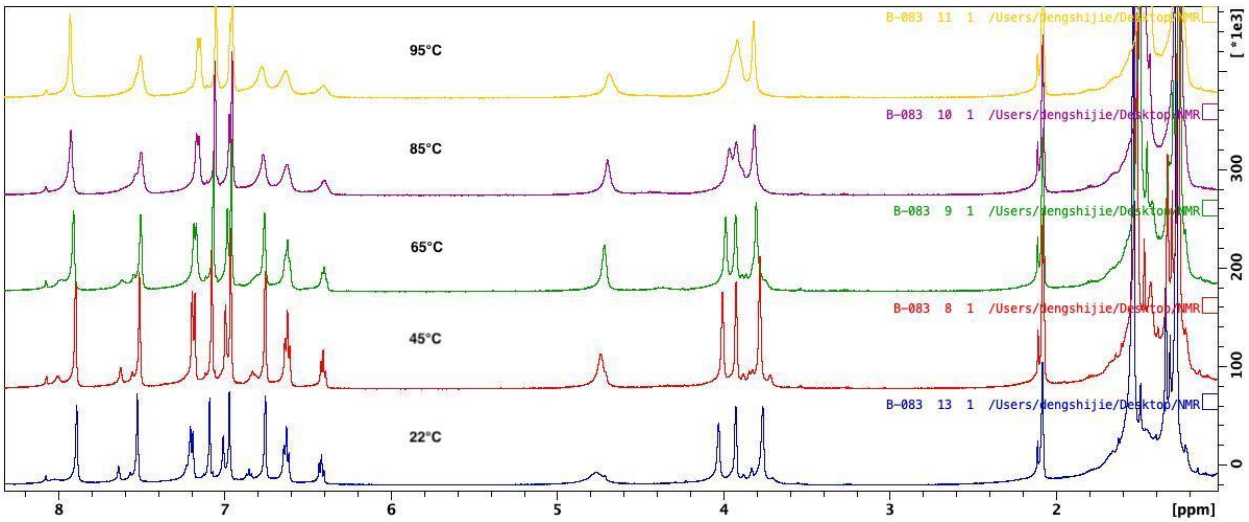

Figure S17. Variable temperature ^{1}H NMR (toluene-d_8, 500 MHz) study of $[(salfen)Y(OPh)]_2$.

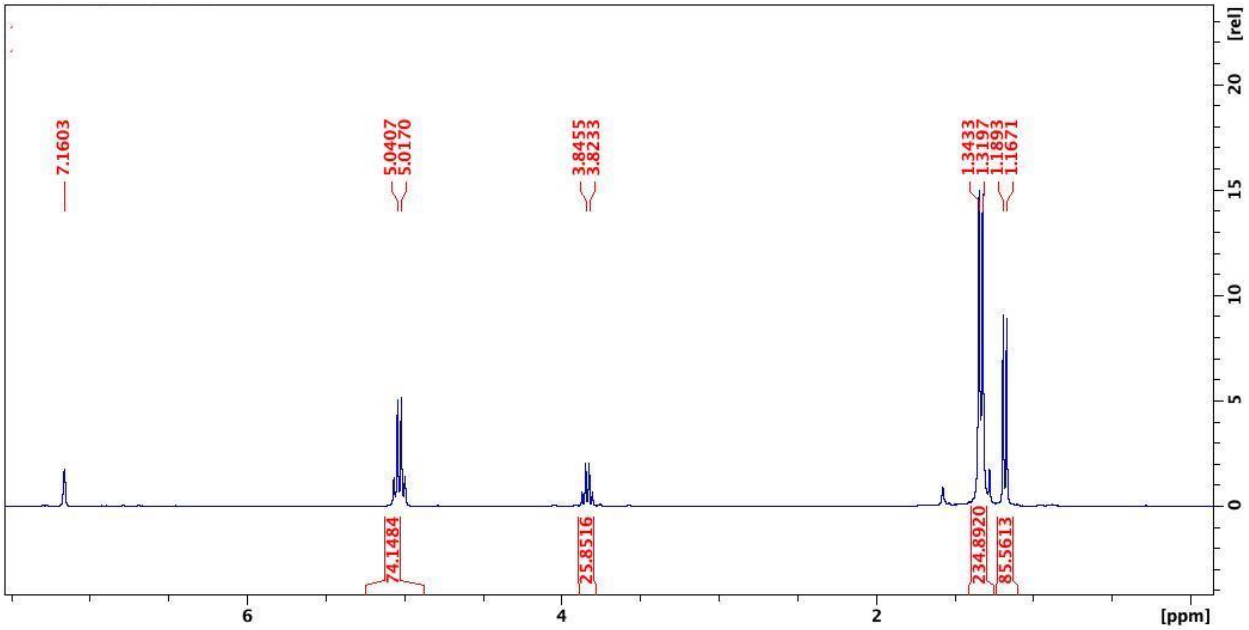

Figure S18. ^{1}H NMR (C_6D_6, 300 MHz, 298 K) spectrum of 200 equivalents of L-lactide polymerization by $[(salfen)Y(OPh)]_2$ (Table 1, entry 1). δ (ppm): 5.04 (q, 1H, C*H*(CH_3)COO, PLA), 3.83 (t, 1H, C*H*(CH_3)COO, LA), 1.34 (d, 3H, CH(C*H*$_3$)COO, PLA), 1.19 (d, 3H, CH(C*H*$_3$)COO, LA).

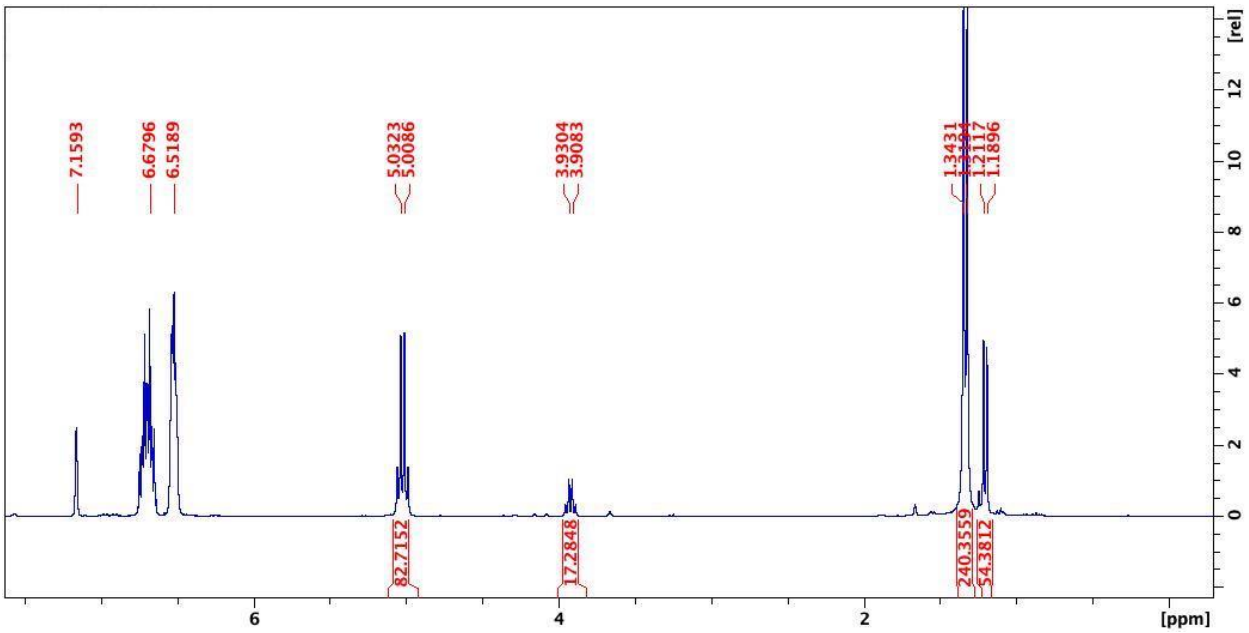

Figure S19. ^{1}H NMR (C_6D_6, 300 MHz, 298 K) spectrum of 200 equivalents of L-lactide polymerization by *in situ* generated $[(salfen)Y(OPh)]_2^+$ (Table 1, entry 2). δ (ppm): 5.03 (q, 1H, C*H*(CH_3)COO, PLA), 3.93 (t, 1H, C*H*(CH_3)COO, LA), 1.34 (d, 3H, CH(C*H*$_3$)COO, PLA), 1.21 (d, 3H, CH(C*H*$_3$)COO, LA).

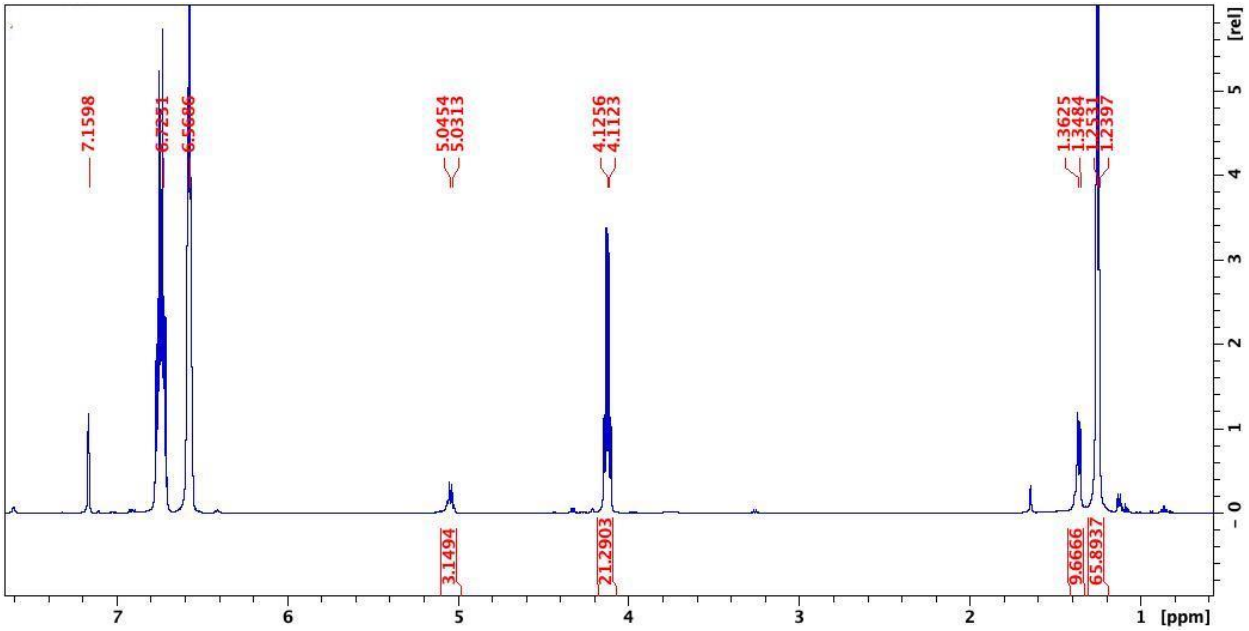

Figure S20. ^{1}H NMR (C_6D_6, 300 MHz, 298 K) spectrum of 200 equivalents of L-lactide polymerization by *in situ* generated $[(salfen)Y(OPh)]_2^{2+}$ (Table 1, entry 3). δ (ppm): 5.03 (q, 1H, C*H*(CH_3)COO, PLA), 4.12 (t, 1H, C*H*(CH_3)COO, LA), 1.36 (d, 3H, CH(C*H*$_3$)COO, PLA), 1.24 (d, 3H, CH(C*H*$_3$)COO, LA).

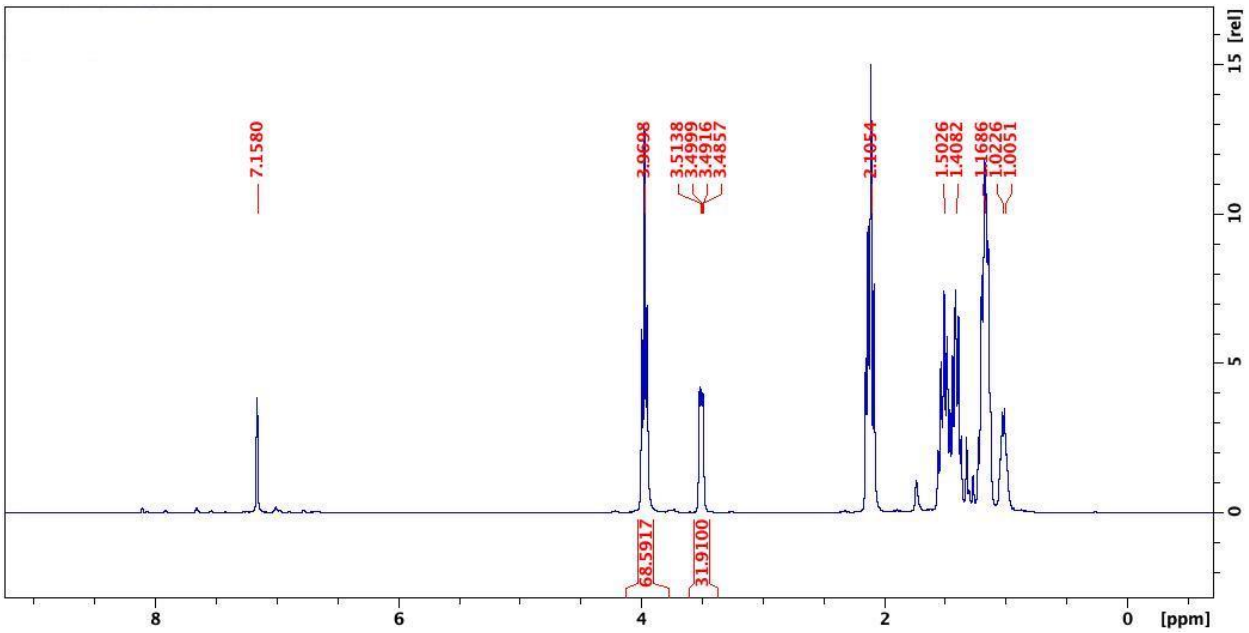

Figure S21. ^{1}H NMR (C_6D_6, 300 MHz, 298 K) spectrum of 200 equivalents of ε-caprolactone polymerization by $[(salfen)Y(OPh)]_2$ (Table 1, entry 4). δ (ppm): 3.97 (t, 2H, COOCH_2, PCL), 3.50 (t, 2H, COOCH_2, CL), 2.10 (t, 2H, CH_2COO, PCL). 1.50 (m, 2H, $COOCH_2CH_2$, PCL) 1.40 (m, 2H, $COOCH_2CH_2CH_2$, PCL), 1.16 (m, 2H, $COOCH_2CH_2CH_2CH_2$, PCL), 1.02. (m, 2H, $COOCH_2CH_2CH_2CH_2$, CL).

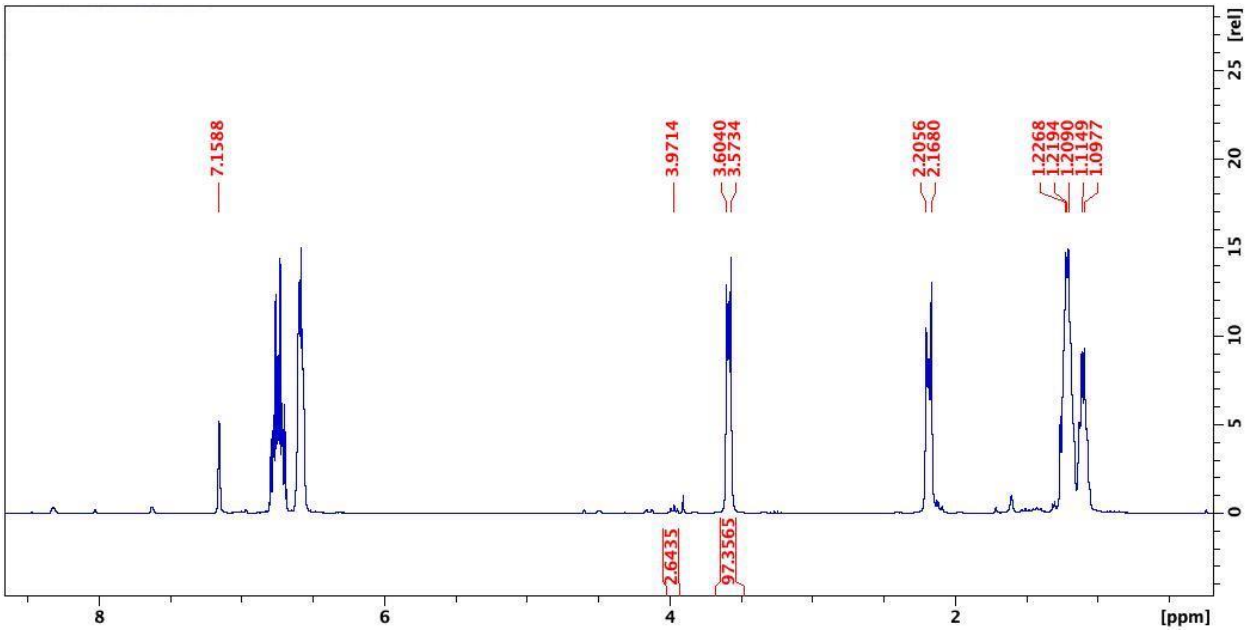

Figure S22. ^{1}H NMR (C_6D_6, 300 MHz, 298 K) spectrum of 200 equivalents of ε-caprolactone polymerization by *in situ* generated $[(salfen)Y(OPh)]_2^+$ (Table 1, entry 5). δ (ppm): 3.97 (t, 2H, COOCH_2, PCL), 3.60 (t, 2H, COOCH_2, CL), 2.20 (t, 2H, CH_2COO, PCL). 1.50 (m, 2H, $COOCH_2CH_2$, PCL) 1.40 (m, 2H, $COOCH_2CH_2CH_2$, PCL), 1.16 (m, 2H, $COOCH_2CH_2CH_2CH_2$, PCL), 1.10. (m, 2H, $COOCH_2CH_2CH_2CH_2$, CL).

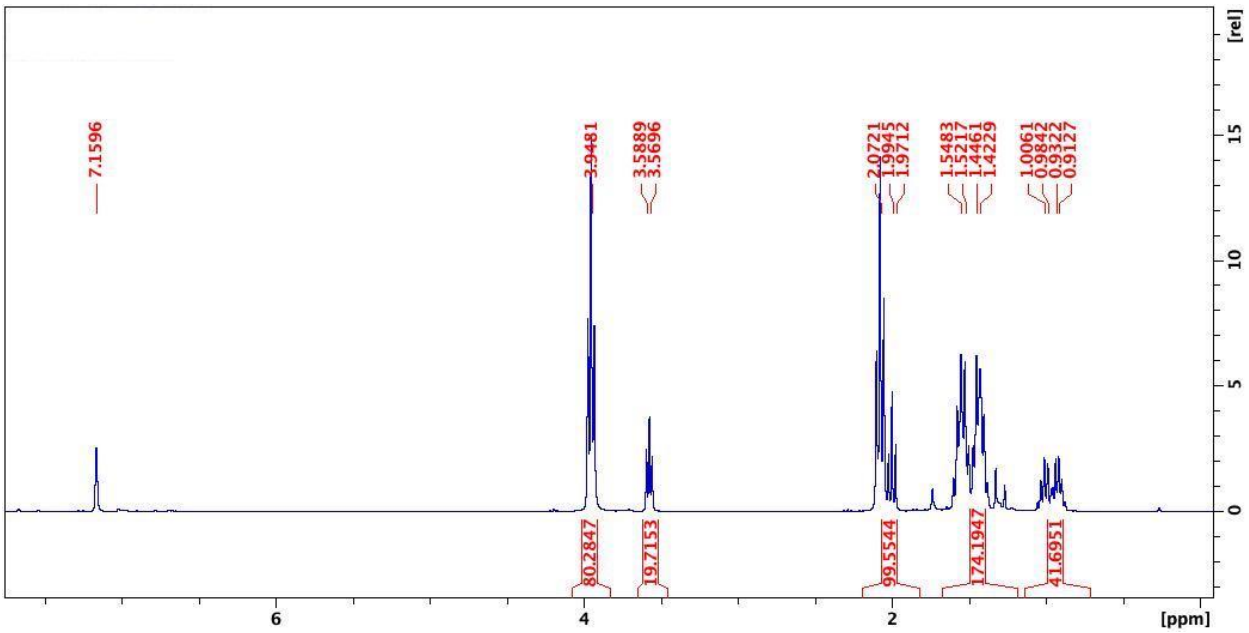

Figure S23. ^{1}H NMR (C_6D_6, 300 MHz, 298 K) spectrum of 200 equivalents of δ-valerolactone polymerization by [(salfen)Y(OPh)]$_2$ (Table 1, entry 7). δ (ppm): 3.95 (t, 2H, COOC*H*$_2$, PVL), 3.57 (t, 2H, COOC*H*$_2$, VL), 2.07 (t, 2H, C*H*$_2$COO, PVL), 1.99 (t, 2H, C*H*$_2$COO, VL), 1.54 (m, 4H, C*H*$_2$C*H*$_2$CH$_2$COO, PVL), 0.96 (m, 4H, C*H*$_2$C*H*$_2$CH$_2$COO, VL).

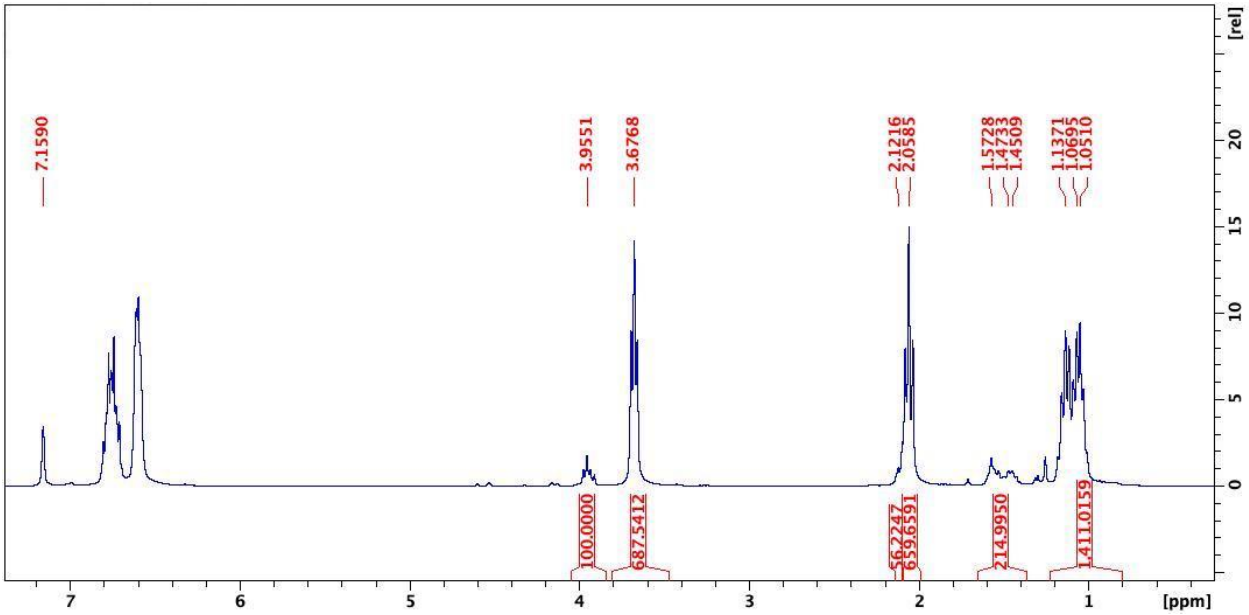

Figure S24. ^{1}H NMR (C_6D_6, 300 MHz, 298 K) spectrum of 200 equivalents of δ-valerolactone polymerization by *in situ* generated [(salfen)Y(OPh)]$_2^+$ (Table 1, entry 8). δ (ppm): 3.95 (t, 2H, COOC*H*$_2$, PVL), 3.57 (t, 2H, COOC*H*$_2$, VL), 2.07 (t, 2H, C*H*$_2$COO, PVL), 1.99 (t, 2H, C*H*$_2$COO, VL), 1.54 (m, 4H, C*H*$_2$C*H*$_2$CH$_2$COO, PVL), 0.96 (m, 4H, C*H*$_2$C*H*$_2$CH$_2$COO, VL).

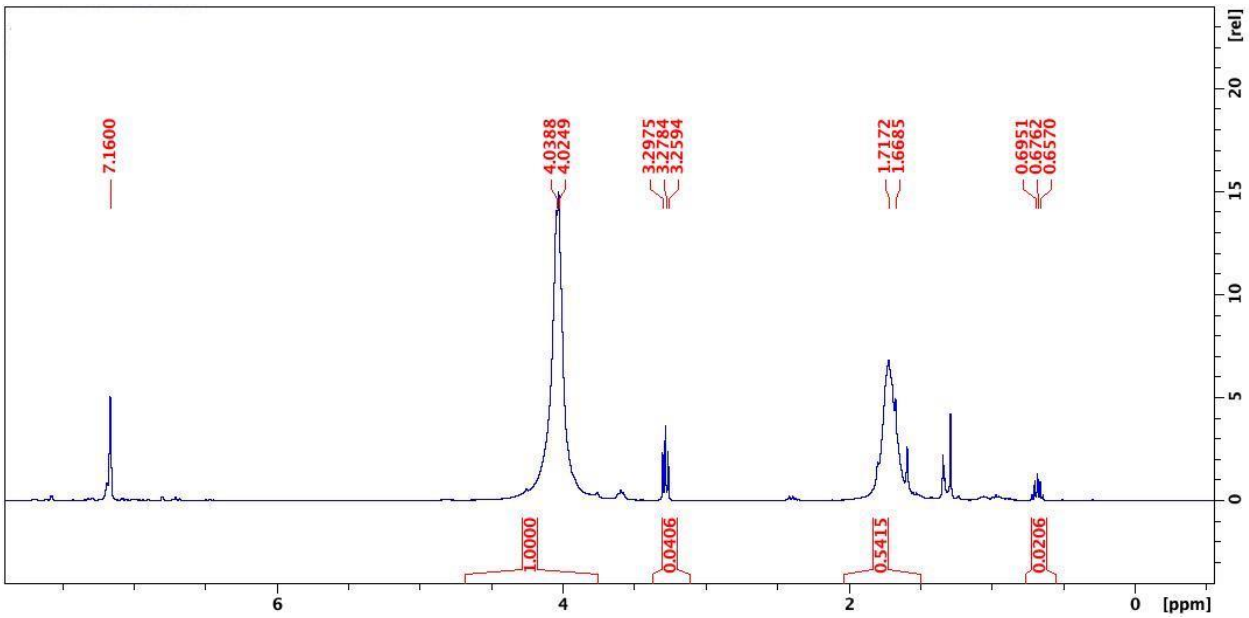

Figure S25. ^{1}H NMR (C_6D_6, 300 MHz, 298 K) spectrum of 200 equivalents of trimethylene carbonate polymerization by $[(salfen)Y(OPh)]_2$ (Table 1, entry 10). δ (ppm): 4.03 (s, 4H, $OCH_2CH_2CH_2O$, PTMC), 3.28 (t, 4H, $OCH_2CH_2CH_2O$, TMC), 1.71 (br, 2H, $OCH_2CH_2CH_2O$, PTMC), 0.70 (m, 2H, $OCH_2CH_2CH_2O$, TMC).

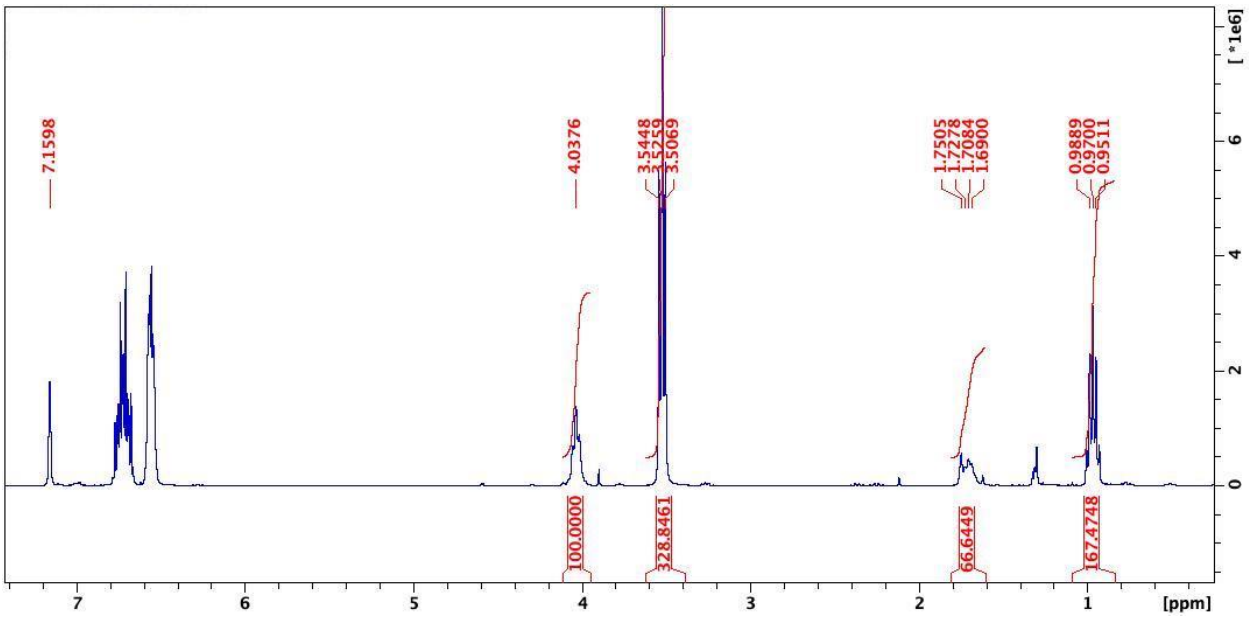

Figure S26. ^{1}H NMR (C_6D_6, 300 MHz, 298 K) spectrum of 200 equivalents of trimethylene carbonate polymerization by *in situ* generated $[(salfen)Y(OPh)]_2^+$ (Table 1, entry 11). δ (ppm): 4.04 (s, 4H, $OCH_2CH_2CH_2O$, PTMC), 3.53 (t, 4H, $OCH_2CH_2CH_2O$, TMC), 1.73 (br, 2H, $OCH_2CH_2CH_2O$, PTMC), 0.97 (m, 2H, $OCH_2CH_2CH_2O$, TMC).

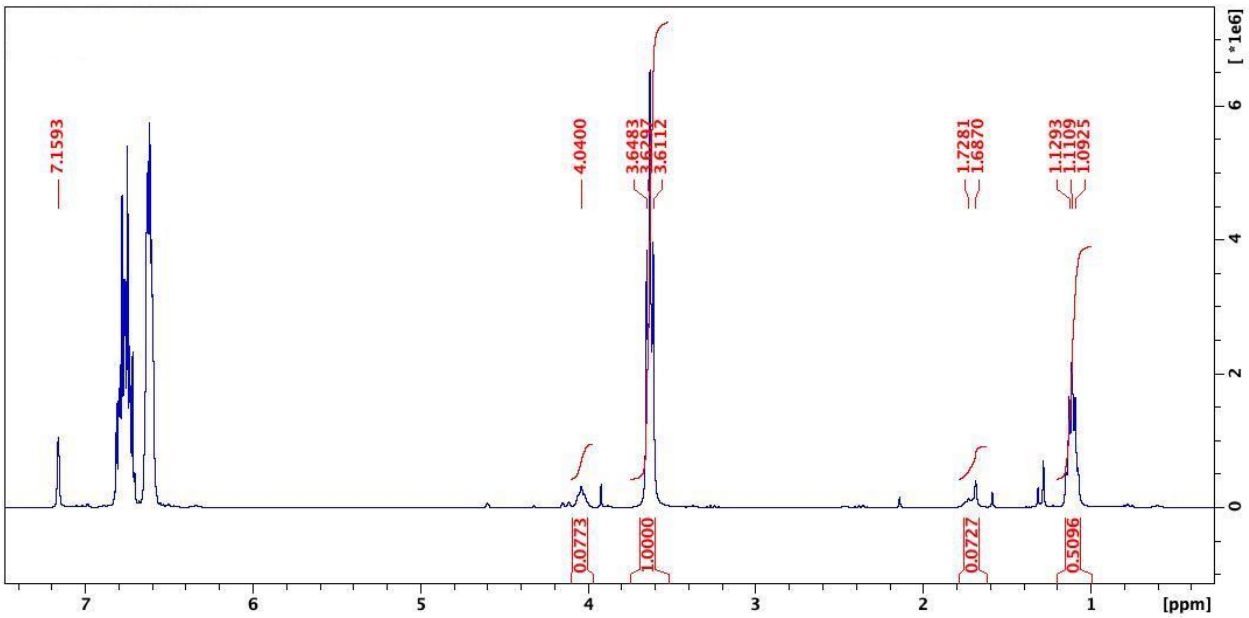

Figure S27. ^{1}H NMR (C_6D_6, 300 MHz, 298 K) spectrum of 200 equivalents of trimethylene carbonate polymerization by *in situ* generated $[(salfen)Y(OPh)]_2^{2+}$ (Table 1, entry 12). δ (ppm): 4.04 (s, 4H, OC*H*$_2$CH$_2$C*H*$_2$O, PTMC), 3.63 (t, 4H, OC*H*$_2$CH$_2$C*H*$_2$O, TMC), 1.73 (br, 2H, OCH$_2$C*H*$_2$CH$_2$O, PTMC), 1.11 (m, 2H, OCH$_2$C*H*$_2$CH$_2$O, TMC).

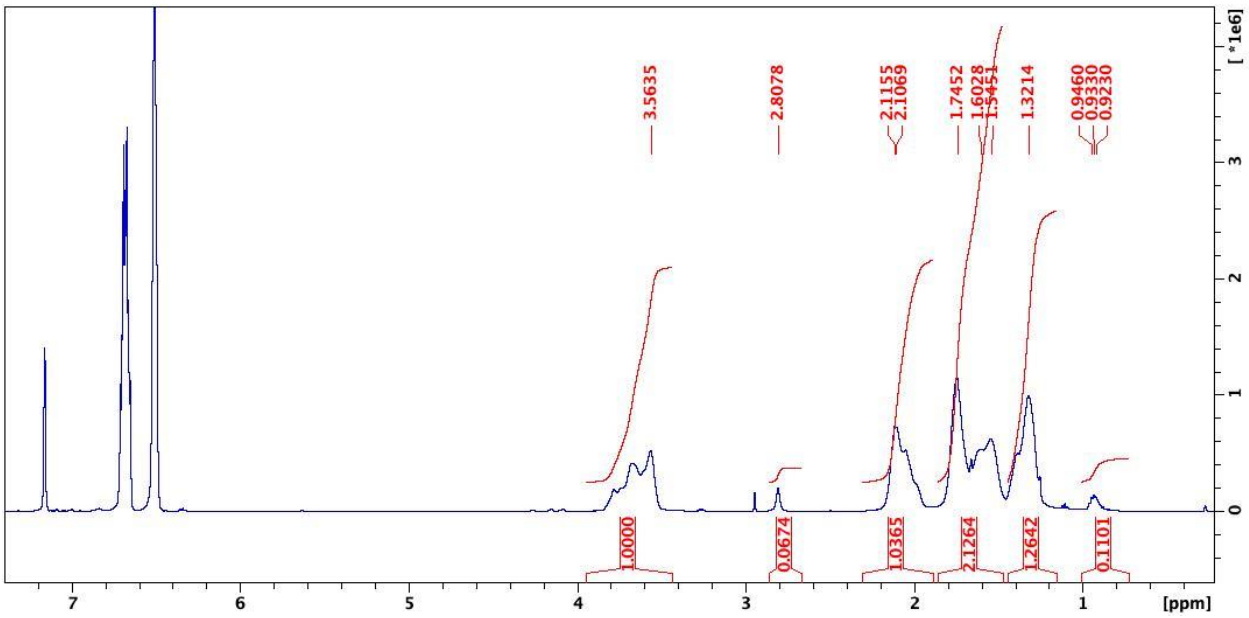

Figure S28. ^{1}H NMR (C_6D_6, 300 MHz, 298 K) spectrum of 200 equivalents of cyclohexene oxide polymerization by *in situ* generated $[(salfen)Y(OPh)]_2^{+}$ (Table 1, entry 14). δ (ppm): 3.56 (br, 2H, CH$_2$CH$_2$C*H*(O), PCHO), 2.80 (br, 2*H*, CH$_2$CH$_2$CH(O), CHO), 2.11 (br, 2H, CH$_2$C*H*$_2$CH(O), PCHO), 1.74 (br, 2H, CH$_2$C*H*$_2$CH(O), PCHO), 1.54 (br, 2H, C*H*$_2$CH$_2$CH(O), PCHO), 1.32 (br, 2H, C*H*$_2$CH$_2$CH(O), PCHO), 0.94 (br, 2H, C*H*$_2$CH$_2$CH(O), CHO).

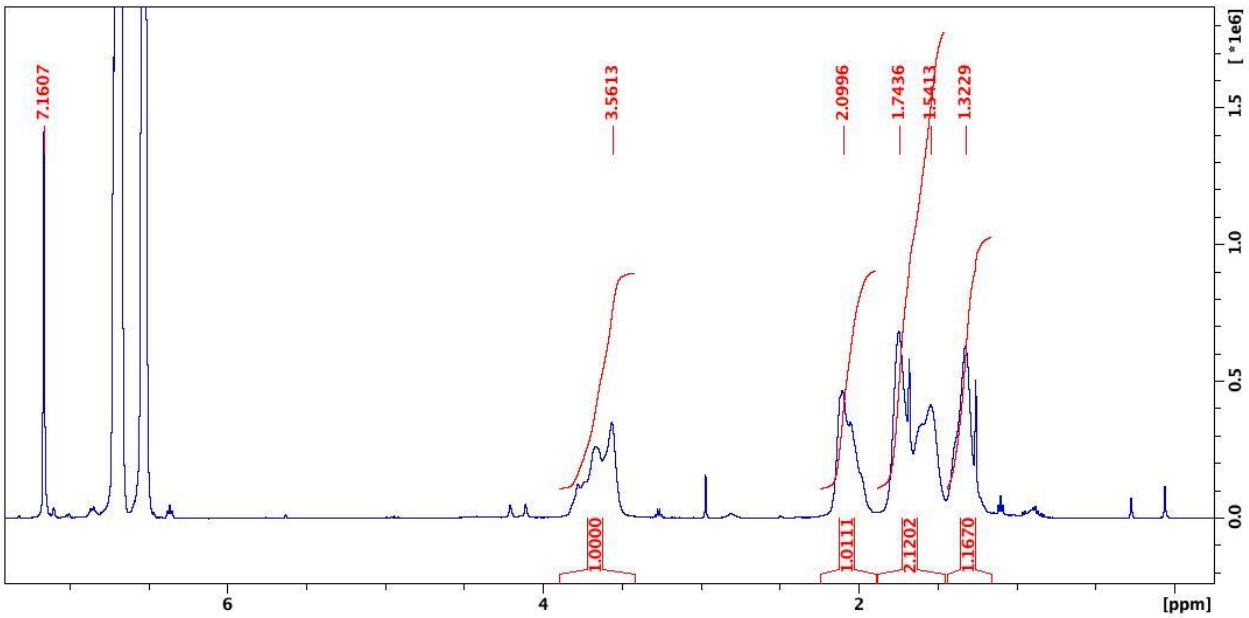

Figure S29. ^{1}H NMR (C_6D_6, 300 MHz, 298 K) spectrum of 200 equivalents of cyclohexene oxide polymerization by *in situ* generated $[(salfen)Y(OPh)]_2^{2+}$ (Table 1, entry 15). δ (ppm): 3.56 (br, 2H, $CH_2CH_2CH(O)$, PCHO), 2.10 (br, 2H, $CH_2CH_2CH(O)$, PCHO), 1.74 (br, 2H, $CH_2CH_2CH(O)$, PCHO), 1.54 (br, 2H, $CH_2CH_2CH(O)$, PCHO), 1.32 (br, 2H, $CH_2CH_2CH(O)$, PCHO).

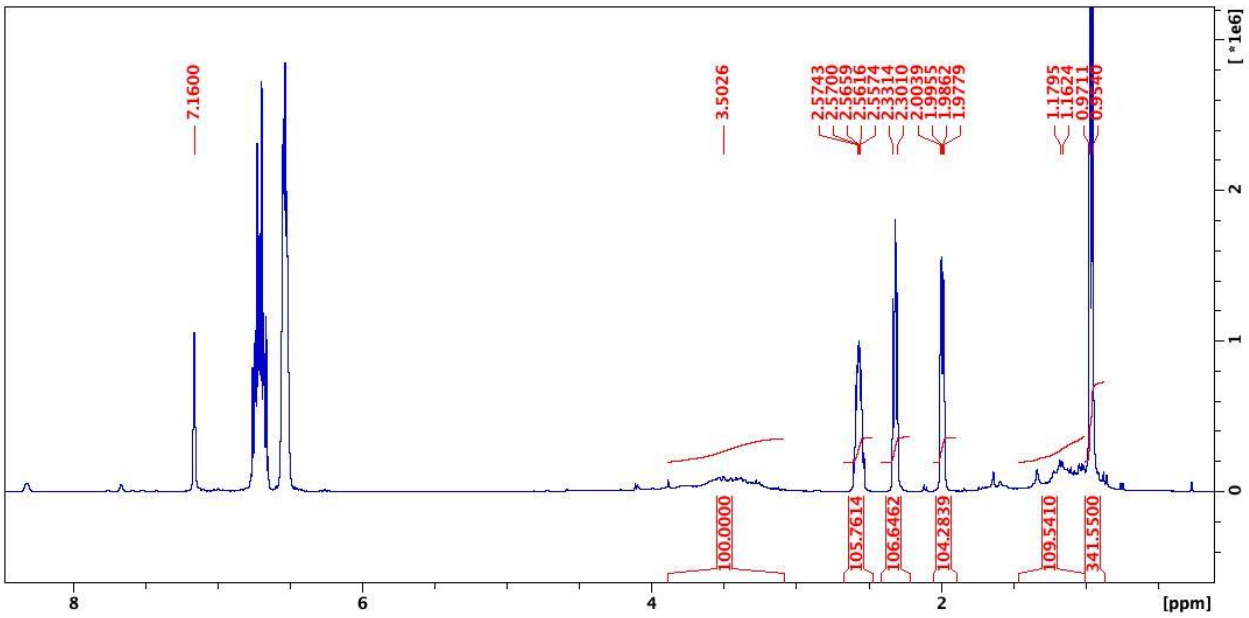

Figure S30. ^{1}H NMR (C_6D_6, 300 MHz, 298 K) spectrum of 200 equivalents of propylene oxide polymerization by *in situ* generated $[(salfen)Y(OPh)]_2^{+}$ (Table 1, entry 17). δ (ppm): 3.50 (br, 3H, $OCH(CH_3)CH_2O$, PPO), 2.57(m, 1H, $OCH(CH_3)CH_2O$, PO), 2.32(t, 1H, $OCH(CH_3)CH_2O$, PO), 2.00(m, 1H, $OCH(CH_3)CH_2O$, PO), 1.17 (br, 3H, $OCH(CH_3)CH_2O$, PPO), 0.97(d, 3H, $OCH(CH_3)CH_2O$, PO).

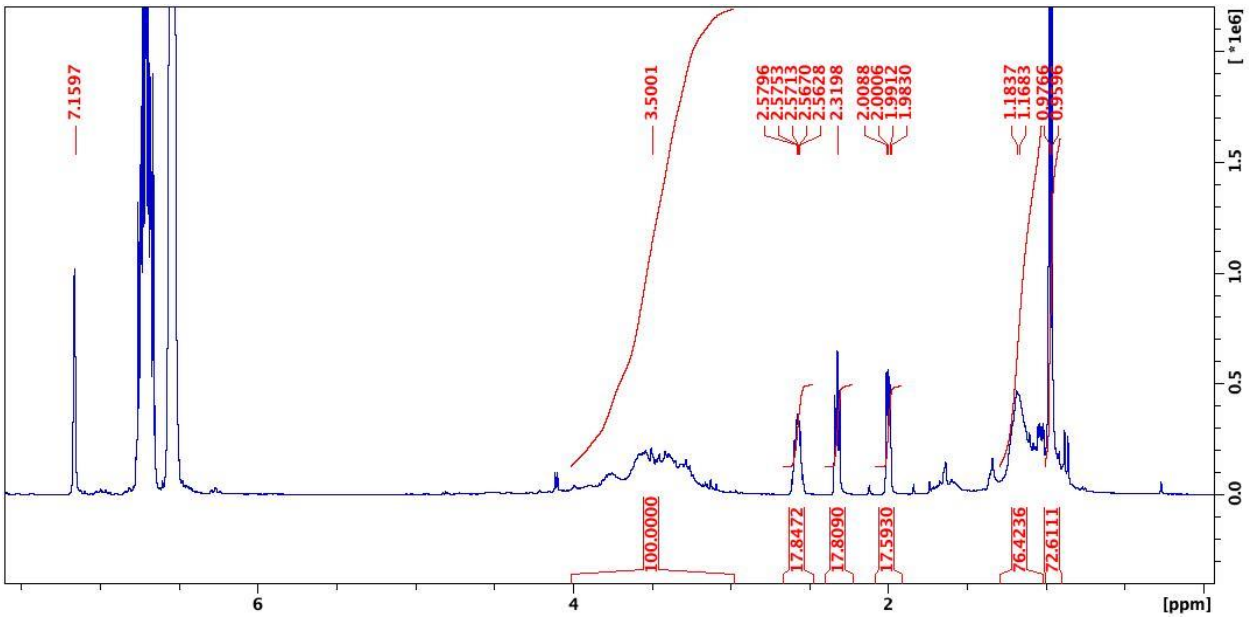

Figure S31. ^{1}H NMR (C_6D_6, 300 MHz, 298 K) spectrum of 200 equivalents of propylene oxide polymerization by *in situ* generated $[(salfen)Y(OPh)]_2^{2+}$ (Table 1, entry 18). δ (ppm): 3.50 (br, 3H, OC*H*(CH_3)C*H*$_2$O, PPO), 2.57(m, 1H, OC*H*(CH_3)CH_2O, PO), 2.32(t, 1H, OCH(CH_3)C*H*$_2$O, PO), 2.00(m, 1H, OCH(CH_3)C*H*$_2$O, PO), 1.18 (br, 3H, OCH(C*H*$_3$)CH_2O, PPO), 0.97(d, 3H, OCH(C*H*$_3$)CH_2O, PO).

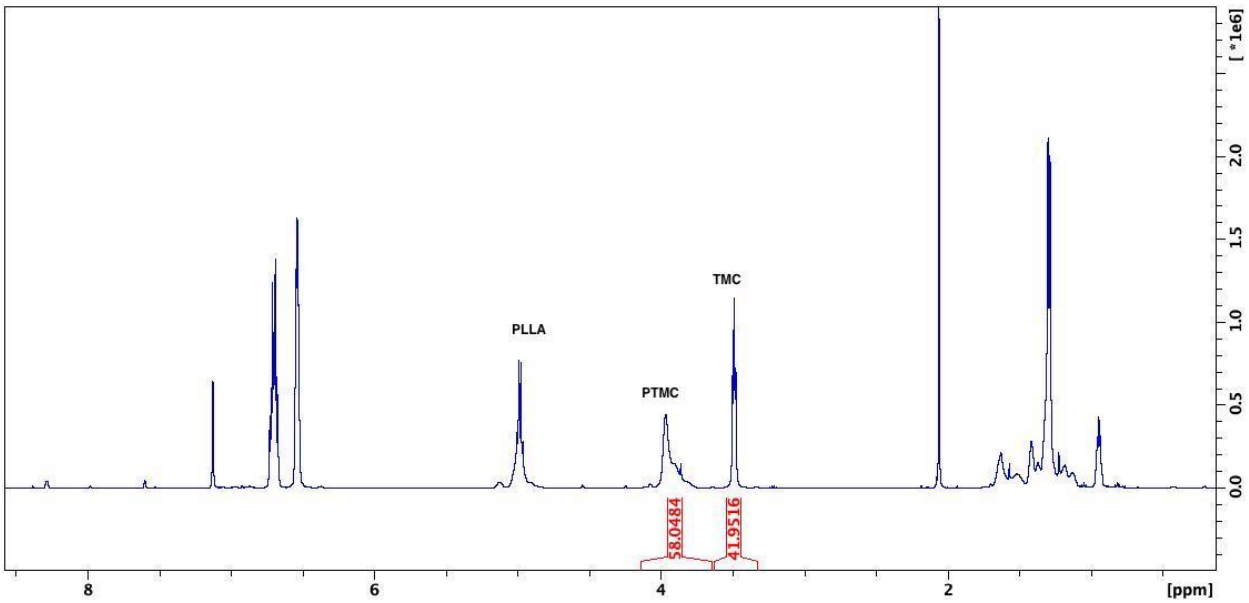

Figure S32. ^{1}H NMR (C_6D_6, 300 MHz, 298 K) spectrum of 200 equivalents of LLA and 200 equivalents of TMC copolymerization (Table 2, entry 2).

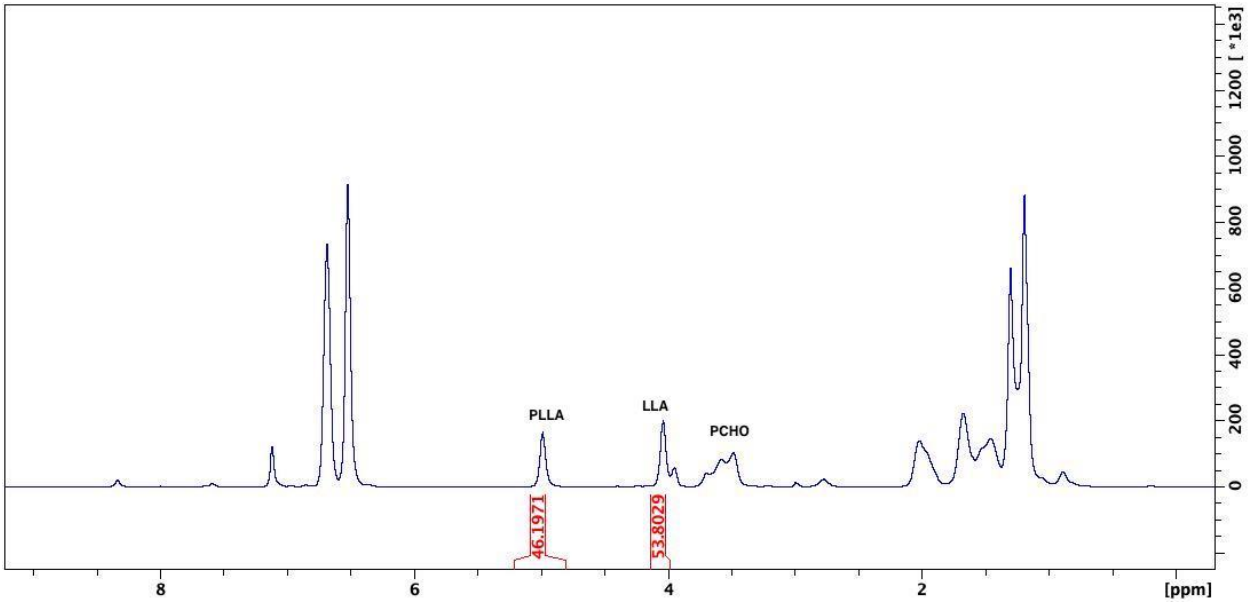

Figure S33. ^{1}H NMR (C_6D_6, 300 MHz, 298 K) spectrum of 200 equivalents of LLA and 200 equivalents of CHO copolymerization (Table 2, entry 3).

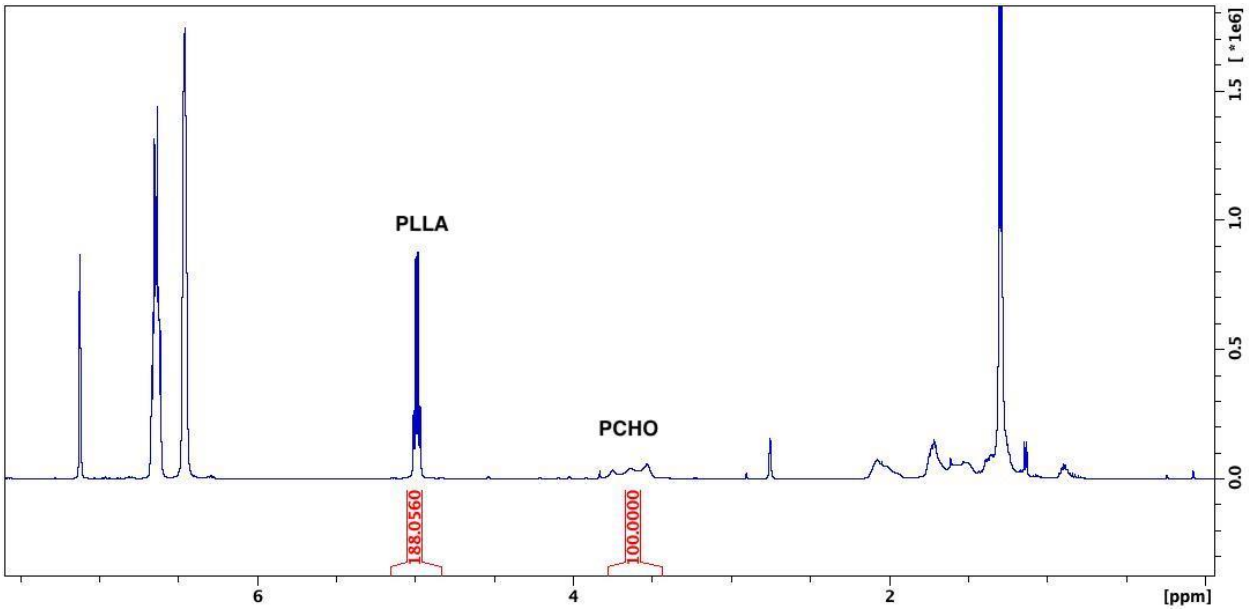

Figure S34. ^{1}H NMR (C_6D_6, 300 MHz, 298 K) spectrum of 200 equivalents of LLA and 200 equivalents of CHO and another 200 equivalents of LLA copolymerization (Table 2, entry 4).

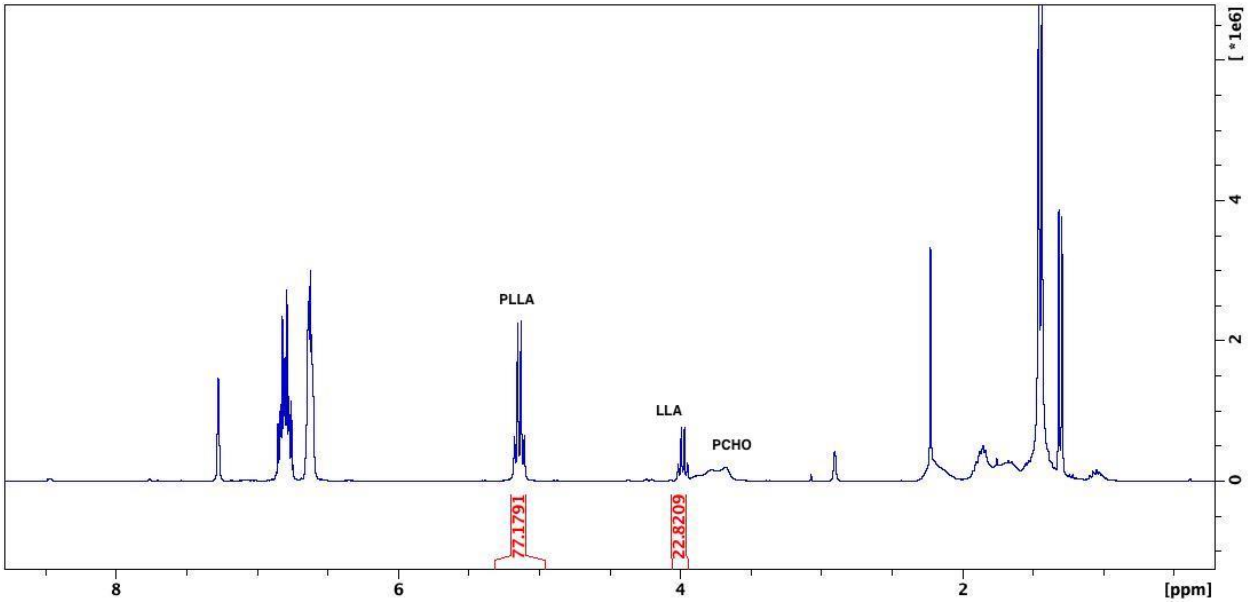

Figure S35. ^{1}H NMR (C_6D_6, 300 MHz, 298 K) spectrum of 200 equivalents of LLA ,200 equivalents of CHO, and another 200 equivalents of LLA copolymerization (Table 2, entry 5).

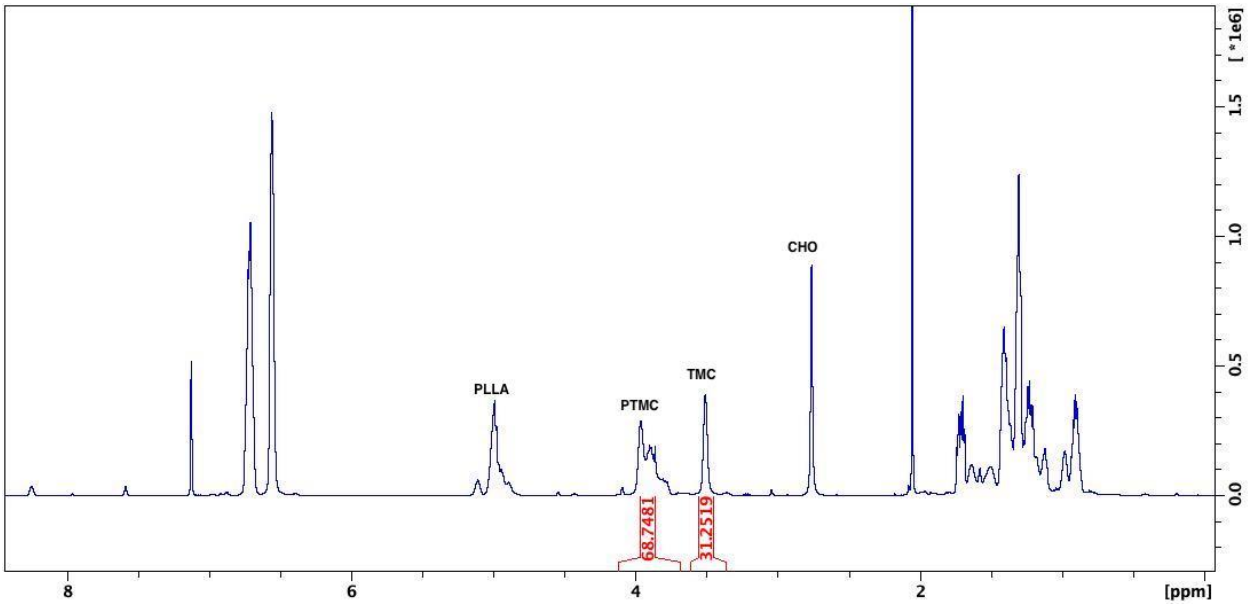

Figure S36. ^{1}H NMR (C_6D_6, 300 MHz, 298 K) spectrum of 200 equivalents of LLA, 200 equivalents of TMC and 200 equivalents of CHO copolymerization (Table 2, entry 6).

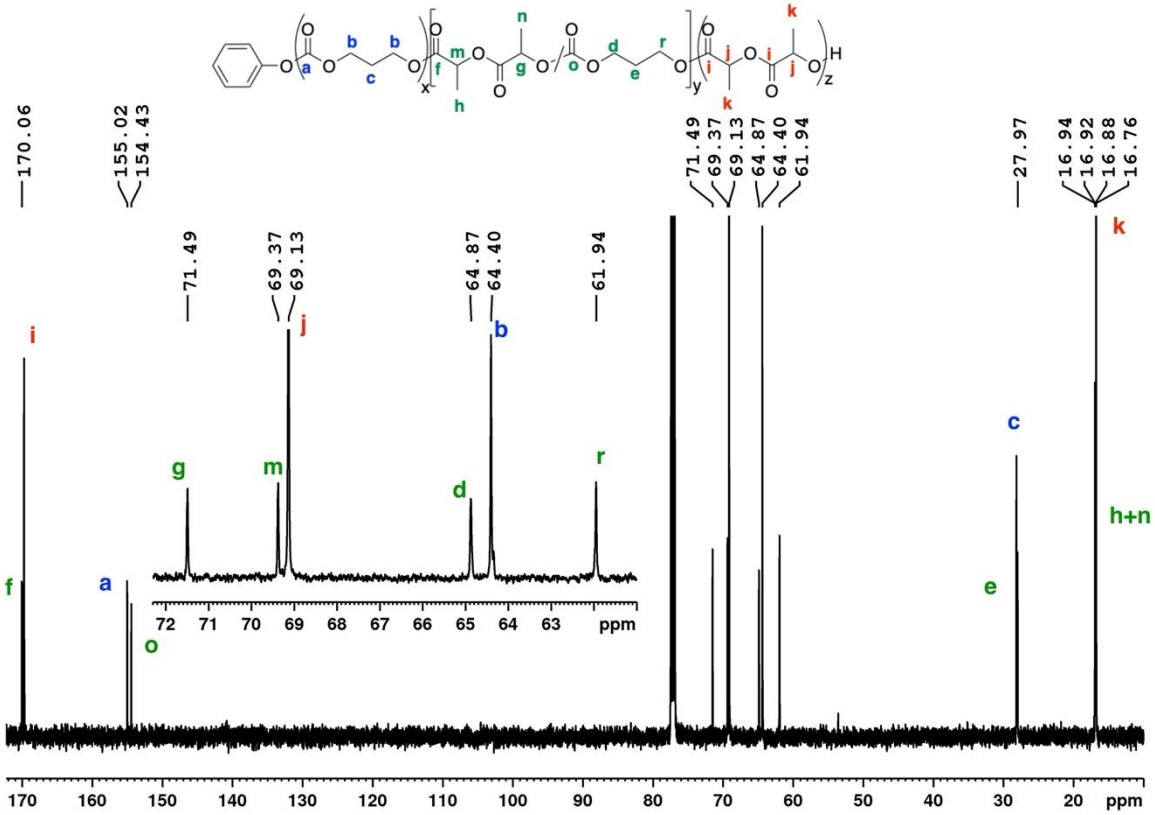

Figure S37. $^{13}C\{^{1}H\}$ NMR ($CDCl_3$, 125 MHz, 298 K) spectrum of 200 equivalents of LLA, 200 equivalents of TMC copolymerization (Table 2, entry 1).

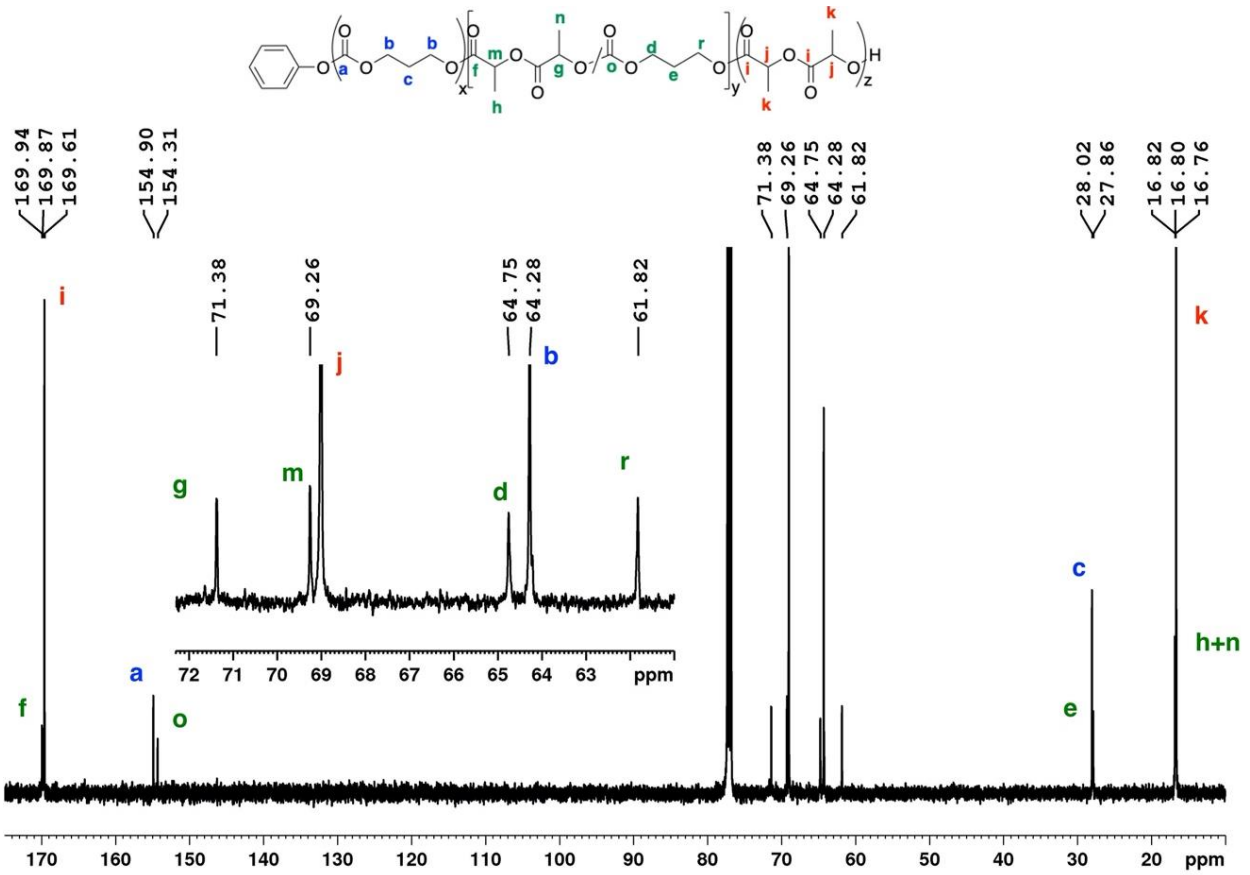

Figure S38. $^{13}C\{^{1}H\}$ NMR ($CDCl_3$, 125 MHz, 298 K) spectrum of 200 equivalents of LLA, 200 equivalents of TMC copolymerization (Table 2, entry 2).

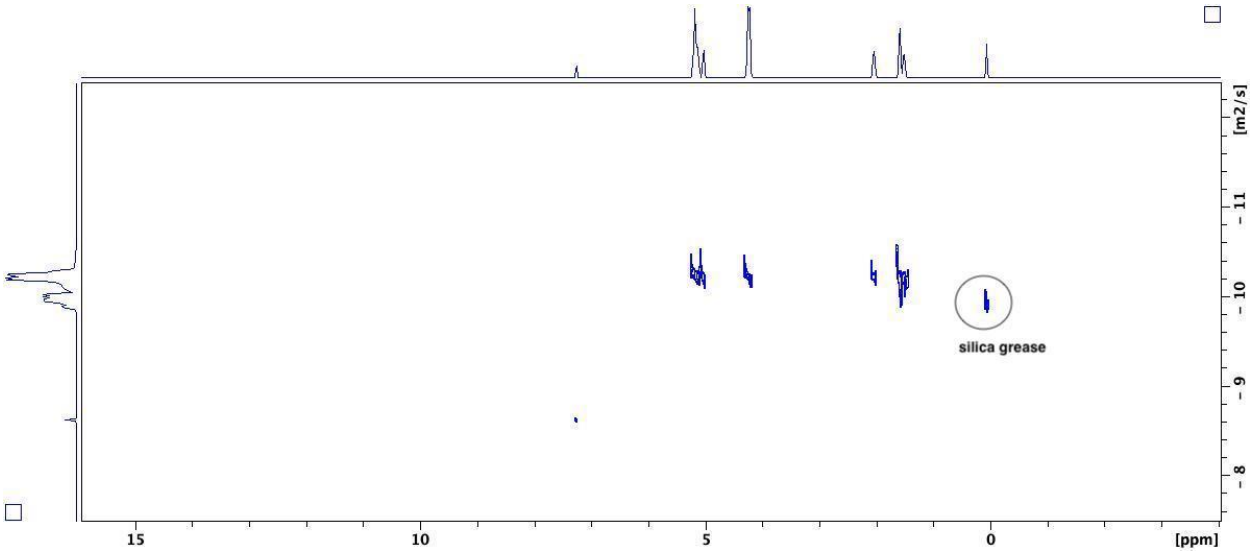

Figure S39. DOSY ($CDCl_3$, 500 MHz, 298 K) of PLLA-PTMC copolymer (Table 2, entry 1).

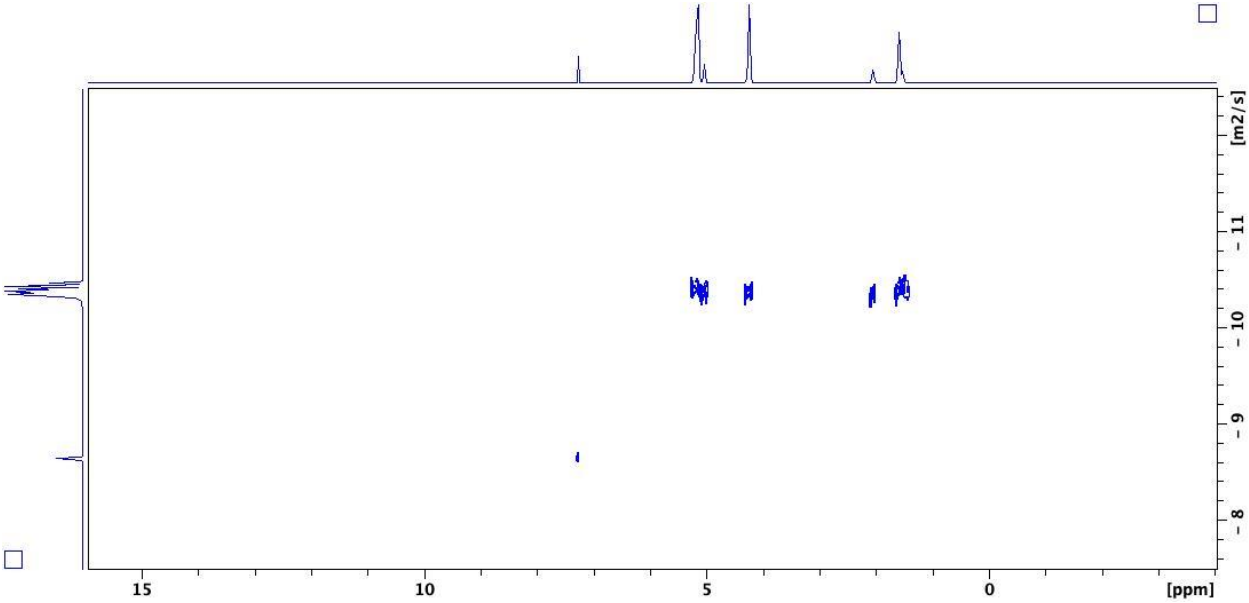

Figure S40. DOSY ($CDCl_3$, 500 MHz, 298 K) of PLLA-PTMC copolymer (Table 2, entry 2).

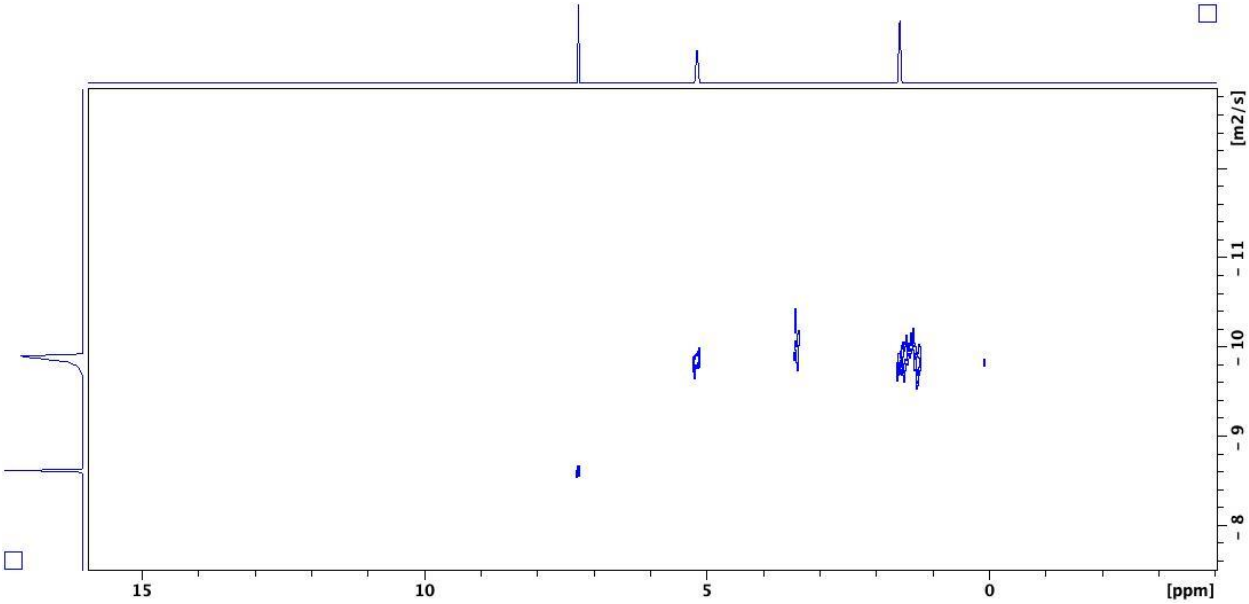

Figure S41. DOSY ($CDCl_3$, 500 MHz, 298 K) of PLLA-PCHO copolymer (Table 2, entry 3).

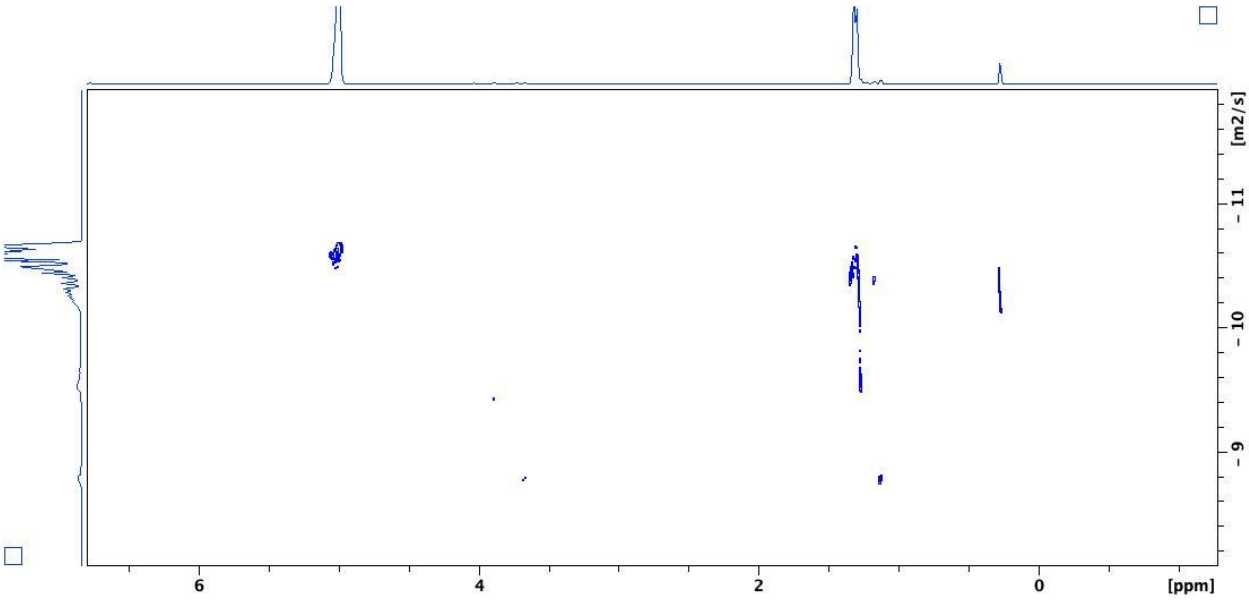

Figure S42. DOSY ($CDCl_3$, 500 MHz, 298 K) of PLLA before quenching with H_2O.

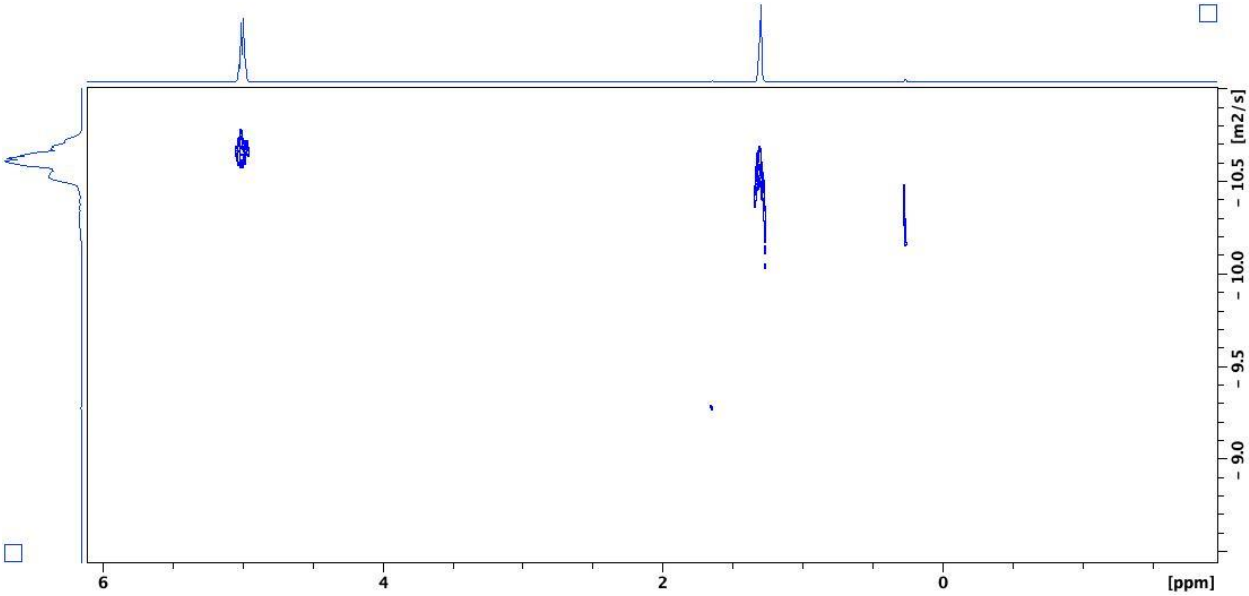

Figure S43. DOSY ($CDCl_3$, 500 MHz, 298 K) of PLLA after quenching with H_2O.

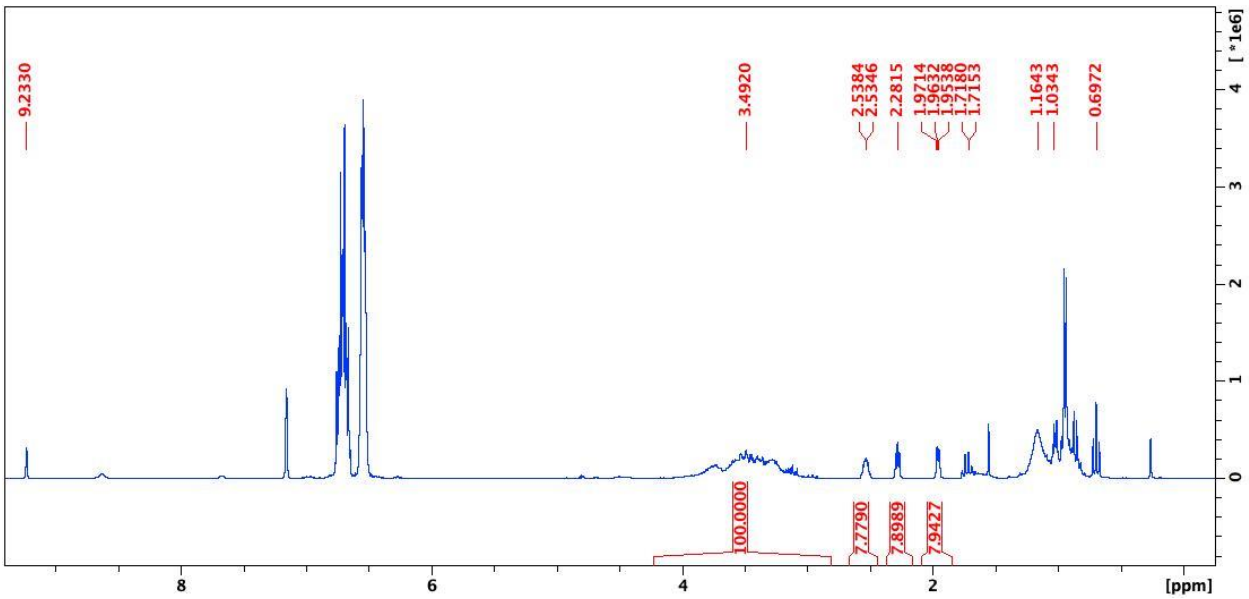

Figure S44. ^{1}H NMR (C_6D_6, 300 MHz, 298 K) spectrum of 200 equivalents of propylene oxide polymerization by ^{Ac}FcBAr^{F} at 298K after 2 hours. δ (ppm): 3.50 (br, 3H, OC*H*(CH_3)C*H*$_2$O, PPO), 2.57(m, 1H, OC*H*(CH_3)CH_2O, PO), 2.32(t, 1H, OCH(CH_3)C*H*$_2$O, PO), 2.00(m, 1H, OCH(CH_3)C*H*$_2$O, PO), 1.18 (br, 3H, OCH(C*H*$_3$)CH_2O, PPO), 0.97(d, 3H, OCH(C*H*$_3$)CH_2O, PO).

SEC traces

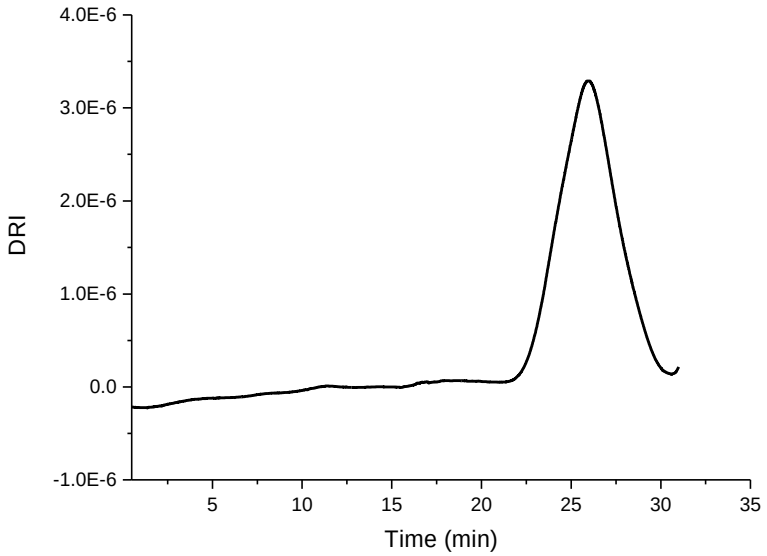

Figure S45. SEC trace for the reaction between 200 equivalents of LLA and $[(salfen)Y(OPh)]_2$ (Table 1, entry 1).

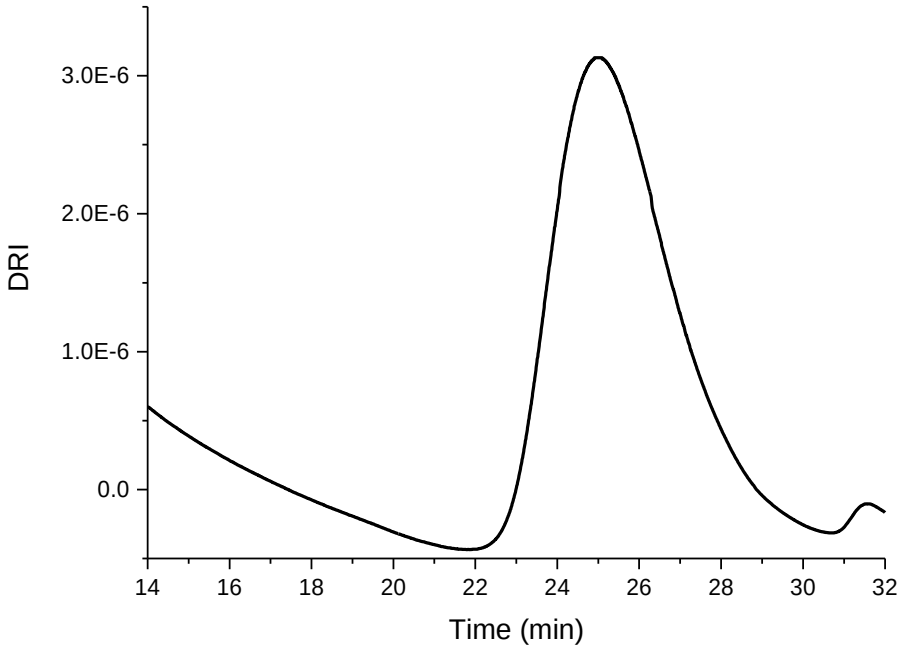

Figure S46. SEC trace for the reaction between 200 equivalents of LLA and *in situ* generated $[(salfen)Y(OPh)]_2^+$ (Table 1, entry 2).

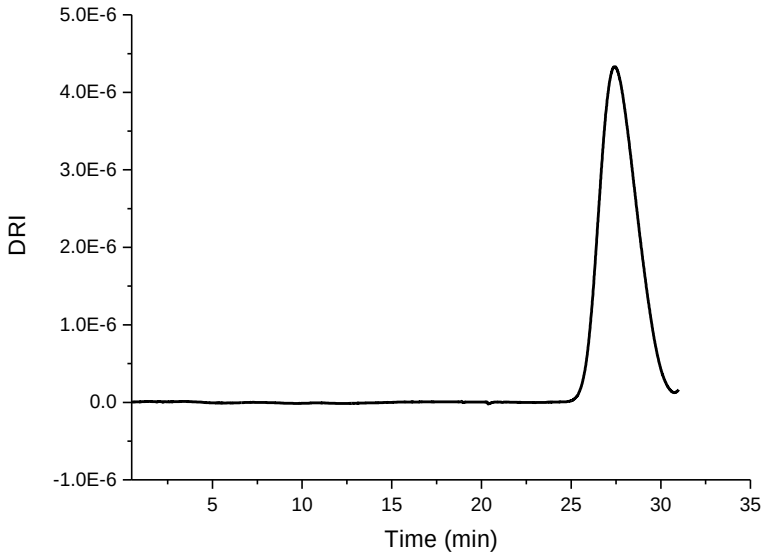

Figure S47. SEC trace for the reaction between 200 equivalents of LLA and *in situ* generated $[(salfen)Y(OPh)]_2^{2+}$ (Table 1, entry 3).

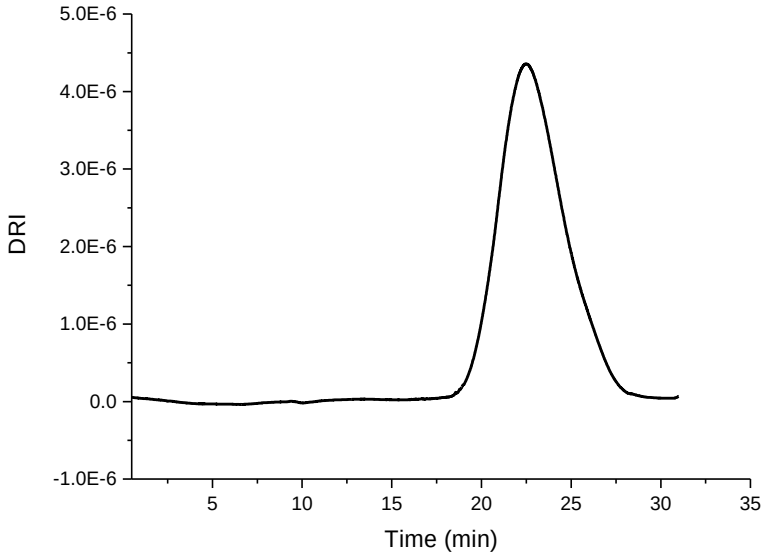

Figure S48. SEC trace for the reaction between 200 equivalents of CL and $[(salfen)Y(OPh)]_2$ (Table 1, entry 4).

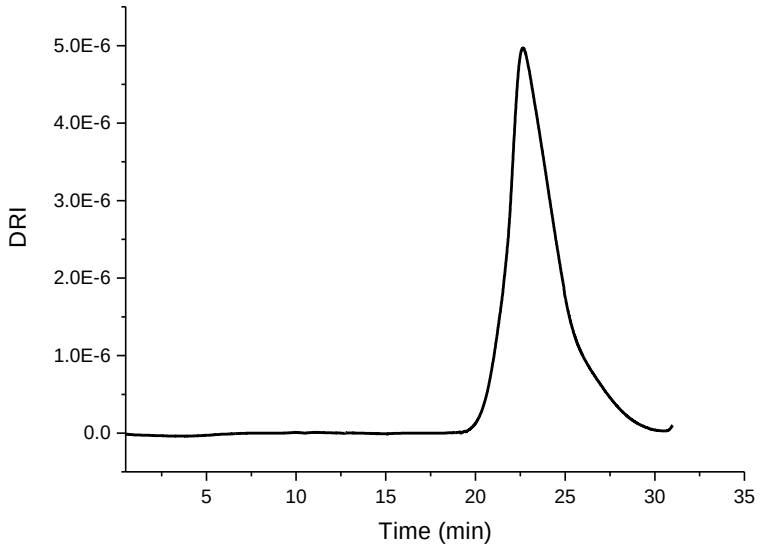

Figure S49. SEC trace for the reaction between 200 equivalents of VL and $[(salfen)Y(OPh)]_2$ (Table 1, entry 7).

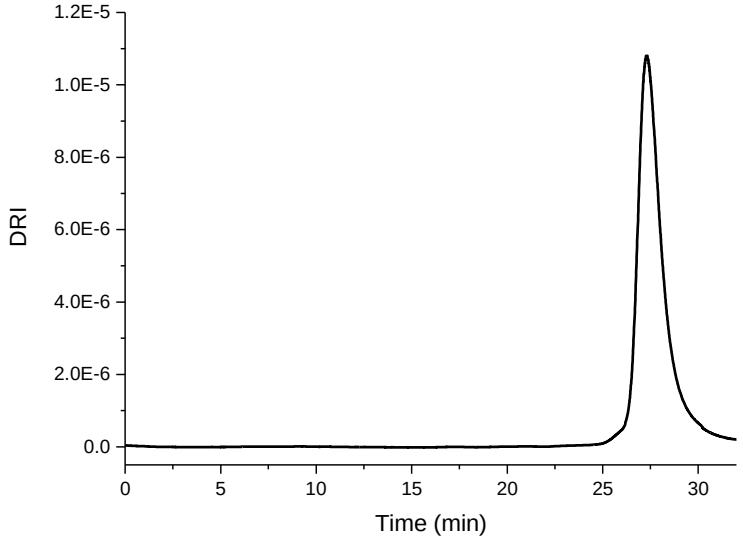

Figure S50. SEC trace for the reaction between 200 equivalents of VL and *in situ* generated $[(salfen)Y(OPh)]_2^+$ (Table 1, entry 8).

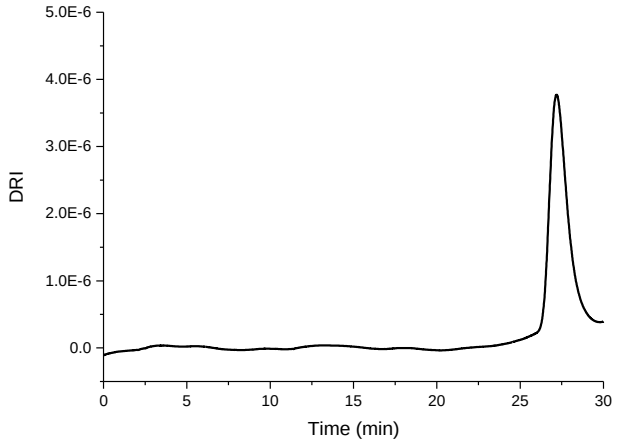

Figure S51. SEC trace for the reaction between 200 equivalents of VL and *in situ* generated $[(salfen)Y(OPh)]_2^{2+}$ (Table 1, entry 9).

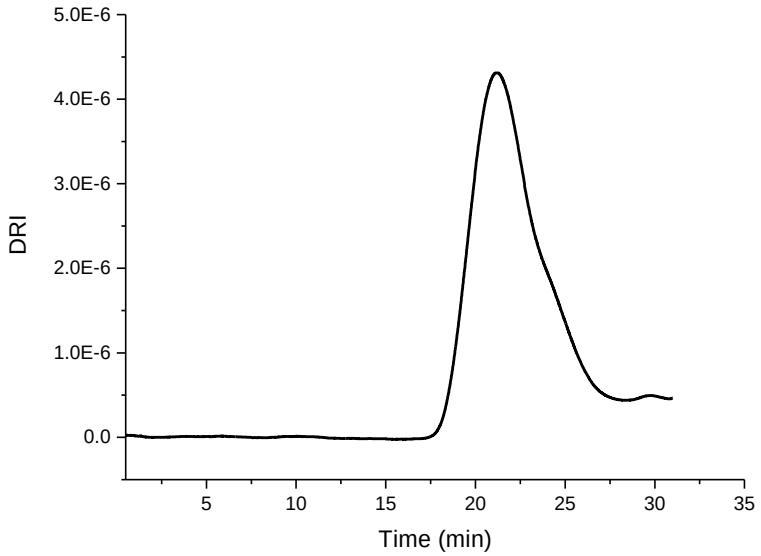

Figure S52. SEC trace for the reaction between 200 equivalents of TMC and $[(salfen)Y(OPh)]_2$ (Table 1, entry 10).

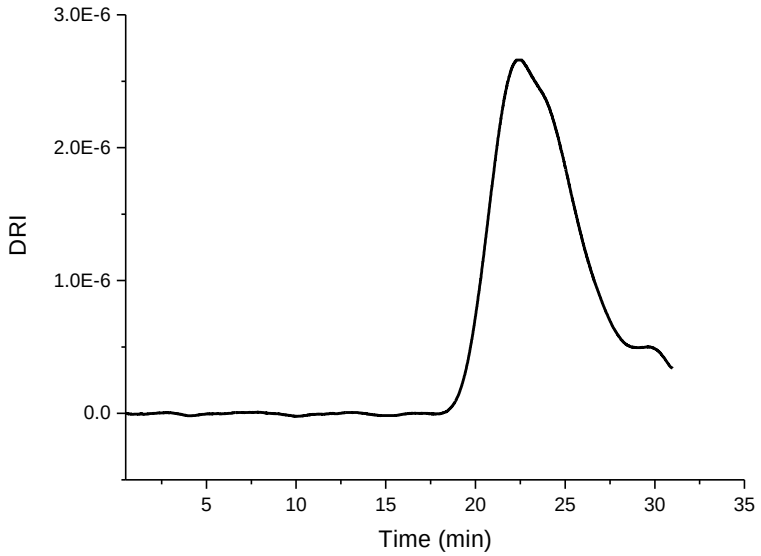

Figure S53. SEC trace for the reaction between 200 equivalents of TMC and *in situ* generated $[(salfen)Y(OPh)]_2^+$ (Table 1, entry 11).

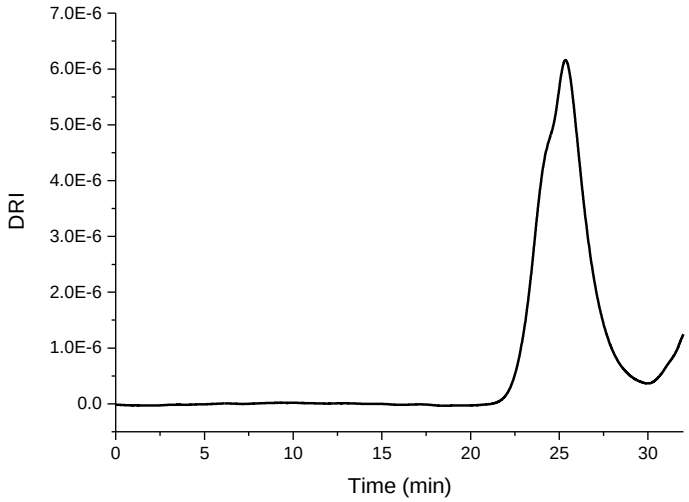

Figure S54. SEC trace for the reaction between 200 equivalents of TMC and *in situ* generated $[(salfen)Y(OPh)]_2^{2+}$ (Table 1, entry 12).

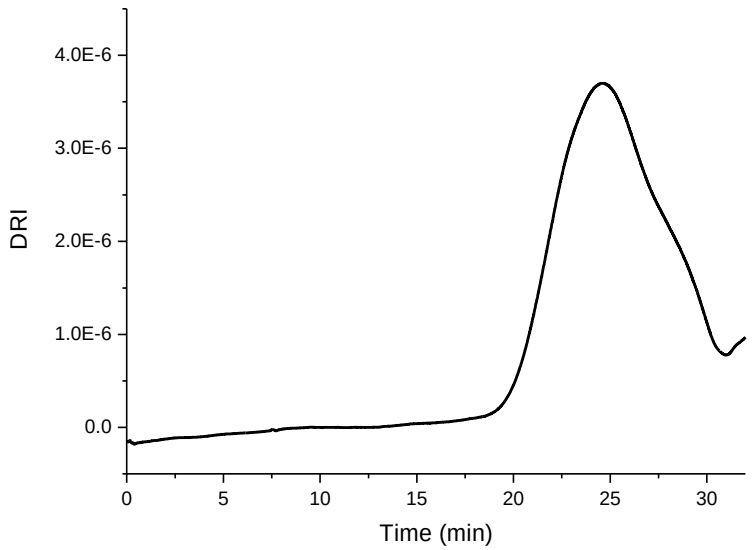

Figure S55. SEC trace for the reaction between 200 equivalents of CHO and *in situ* generated $[(salfen)Y(OPh)]_2^+$ (Table 1, entry 14).

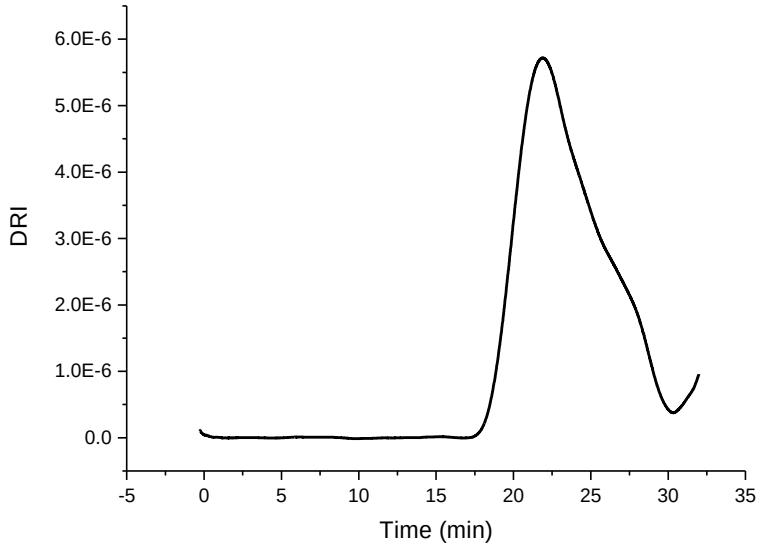

Figure S56. SEC trace for the reaction between 200 equivalents of CHO and *in situ* generated $[(salfen)Y(OPh)]_2^{2+}$ (Table 1, entry 15).

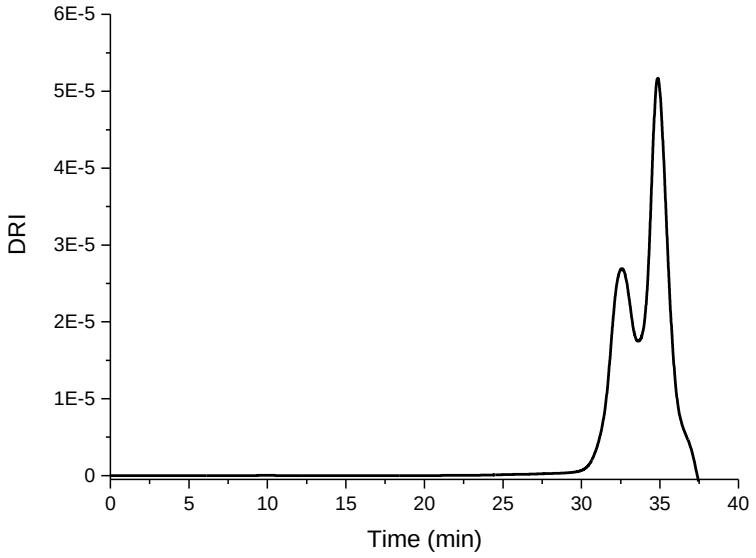

Figure S57. SEC trace for the reaction between 200 equivalents of PO and *in situ* generated $[(salfen)Y(OPh)]_2^+$ (Table 1, entry 17).

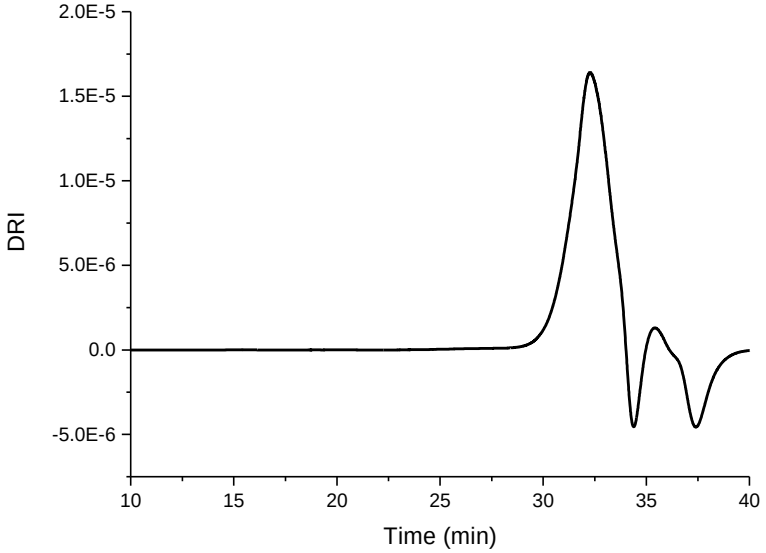

Figure S58. SEC trace for the reaction between 200 equivalents of PO and *in situ* generated $[(salfen)Y(OPh)]_2^{2+}$ (Table 1, entry 18).

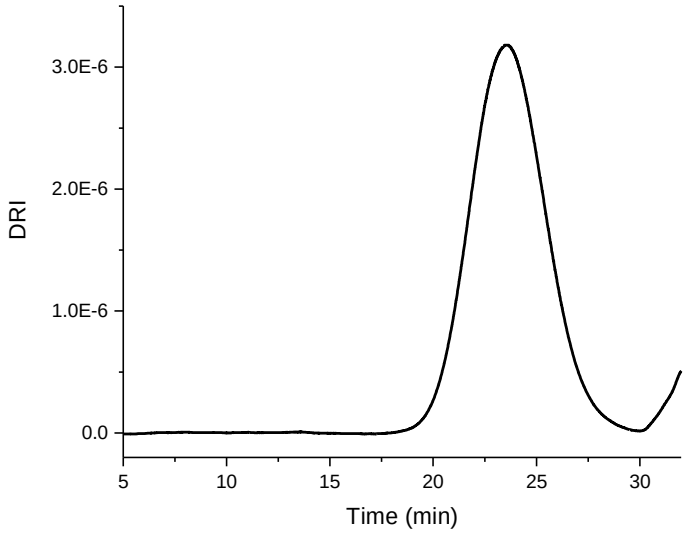

Figure S59. SEC trace for PLLA-PTMC copolymer (Table 2, entry 1).

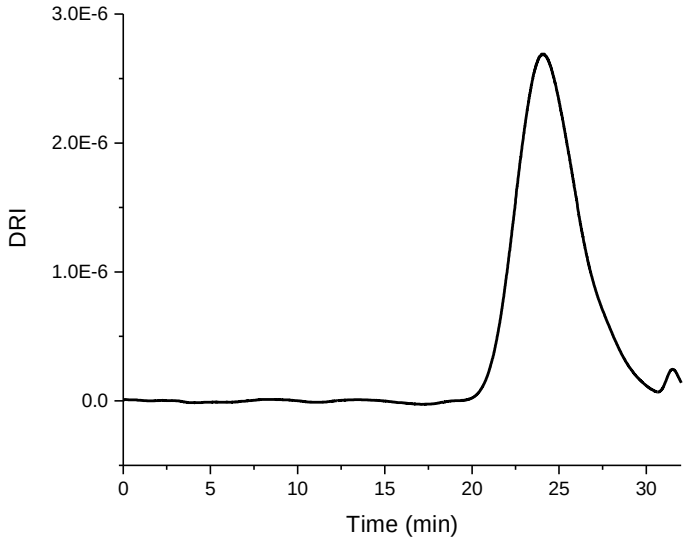

Figure S60. SEC trace for PLLA-PTMC copolymer (Table 2, entry 2).

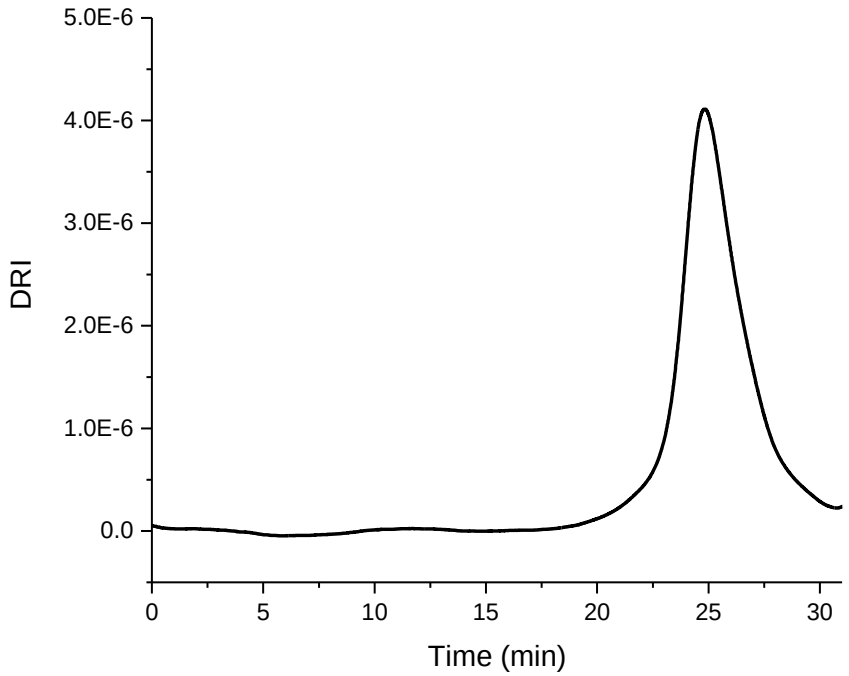

Figure S61. SEC trace for PLLA-PCHO copolymer (Table 2, entry 3).

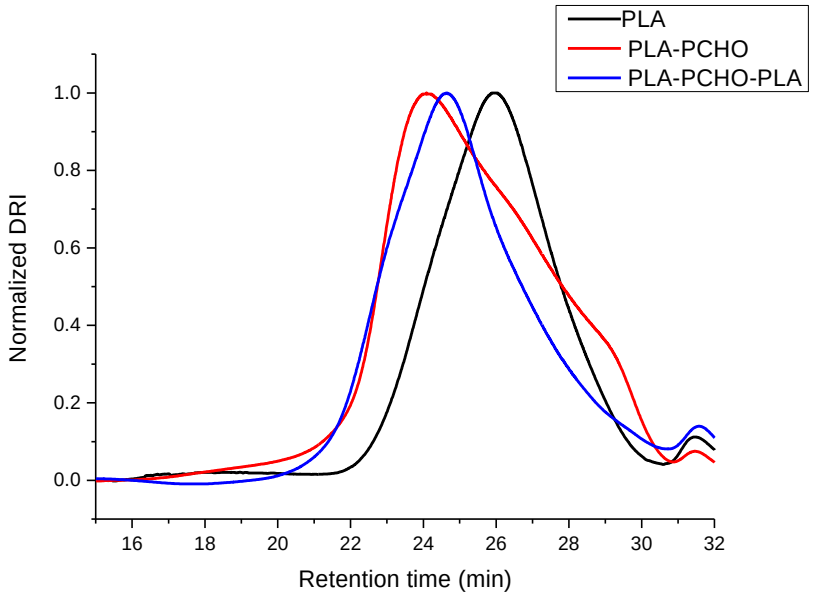

Figure S62. SEC traces corresponding to the stepwise preparation of PLLA-PCHO-PLLA (Table 2, entry 4).

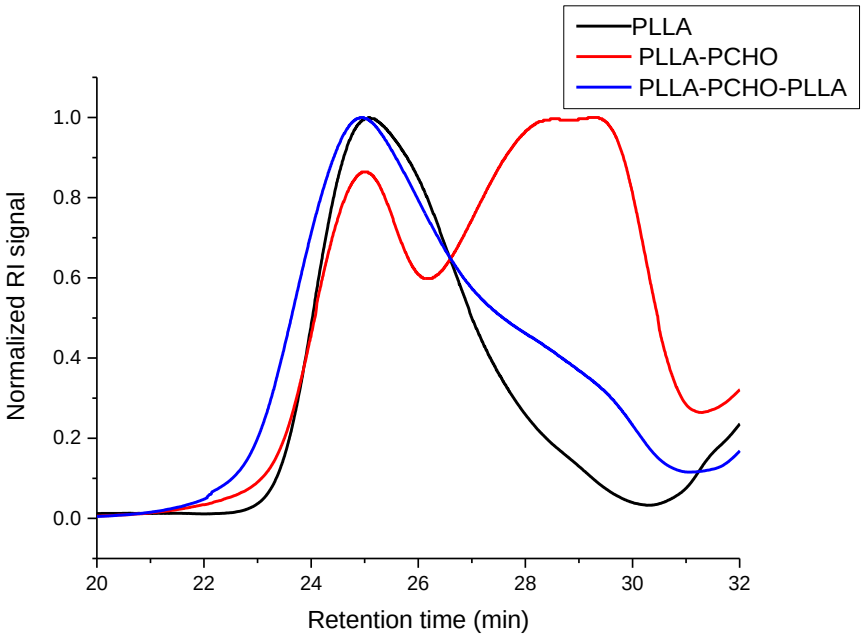

Figure S63. SEC traces corresponding to the stepwise preparation of PLLA-PCHO-PLLA (Table 2, entry 5).

Table S1. Replication of homopolymerization results

Entry	Monomer[b]	Cat.[c]	Time	Conv. (%)	$M_{n,calc}$[d] (kDa)	$M_{n,exp}$[e] (kDa)	Đ
1	LLA	red	0.6 h	92	13	17	1.26
2	LLA	ox^{+}	5 h	84	12	29	1.20
3	LLA	ox^{2+}	24 h	31	4.4	7.9	1.27
4	CL	red	21 h	81	8.3	83	1.59
5	CL	ox^{+}	24 h	11	N/A		
6	CL	ox^{2+}	24 h	0	N/A		
7	VL	red	10 h	82	N/A		
8	VL	ox^{+}	24 h	32	N/A		
9	VL	ox^{2+}	24 h	7	N/A		
10	TMC	red	25 h	99	10	118	1.50
11	TMC	ox^{+}	72 h	84	8.6	16	1.33
12	TMC	ox^{2+}	72 h	40	N/A		
13	CHO	red	24 h	0	N/A		
14	CHO	ox^{+}	5 min	99	9.7	27	2.5
15	CHO	ox^{2+}	5 min	99	9.7	60	3.5
16[f]	PO	red	24 h	0	N/A		
17[f]	PO	ox^{+}	48 h	25	N/A		
18[f]	PO	ox^{2+}	49 h	56	3.3	300	1.39

[a] All polymerization reactions were performed with 2.5 μmol precatalyst, 0.6 mL of C_6D_6 as the solvent, 200 equivalents of monomer, at ambient temperature unless otherwise mentioned; conversions were determined by ^{1}H NMR spectroscopy. [b] LLA stands for L-lactide, CL stands for ε-caprolactone, VL stands for δ-valerolactone, TMC stands for 1,3-trimethylene carbonate, CHO stands for cyclohexene oxide, and PO stands for propylene oxide. [c] "red" represents $[(salfen)Y(OPh)]_2$, "ox^{+}" represents *in situ* generated $[(salfen)Y(OPh)]_2^{+}$, and "ox^{2+}" represents *in situ* generated $[(salfen)Y(OPh)]_2^{2+}$. [d] $M_{n,calc}$ is calculated based on initiation from both phenoxide groups, $M_{n,calc} = M_{monomer} \times 100 \times$ conversion. [e] $M_{n,exp}$ were determined by SEC measurements. [f] Polymerization was conducted at 80 °C.

TGA traces

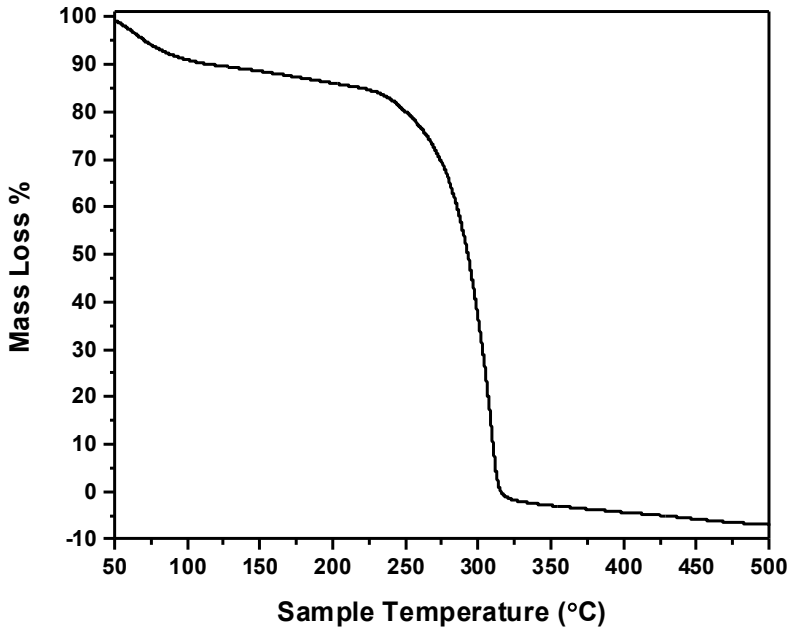

Figure S64. TGA trace for PLLA-PTMC copolymer (Table 2, entry 1)

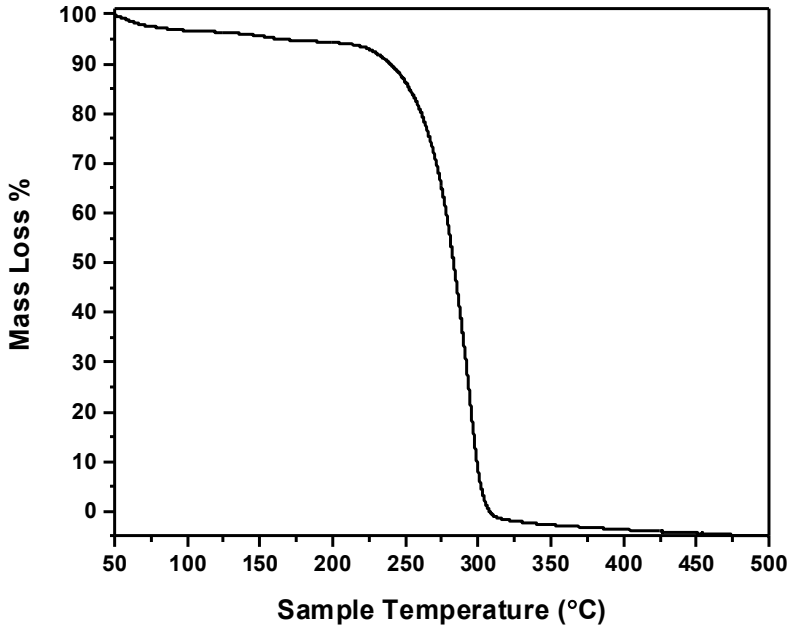

Figure S65. TGA trace for PLLA-PTMC copolymer (Table 2, entry 2).

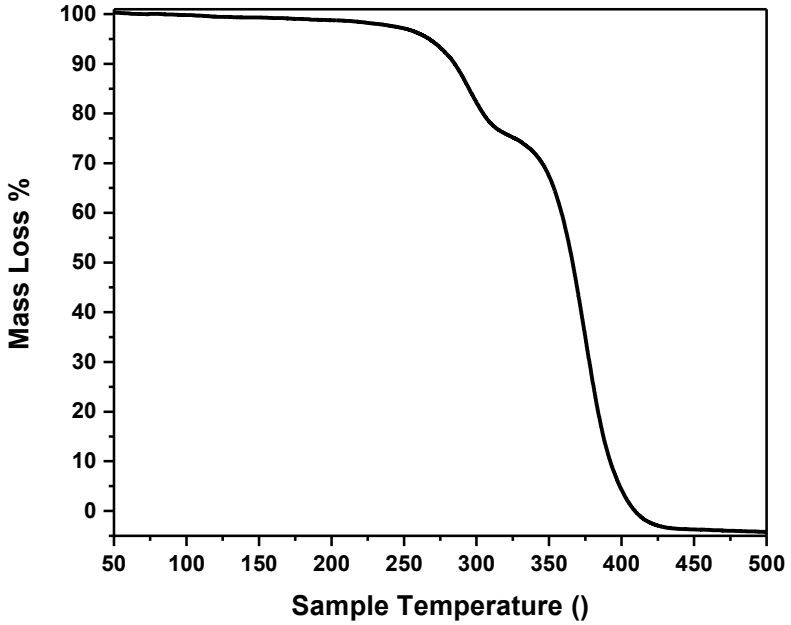

Figure S66. TGA trace for PLLA-PCHO copolymer (Table 2, entry 3).

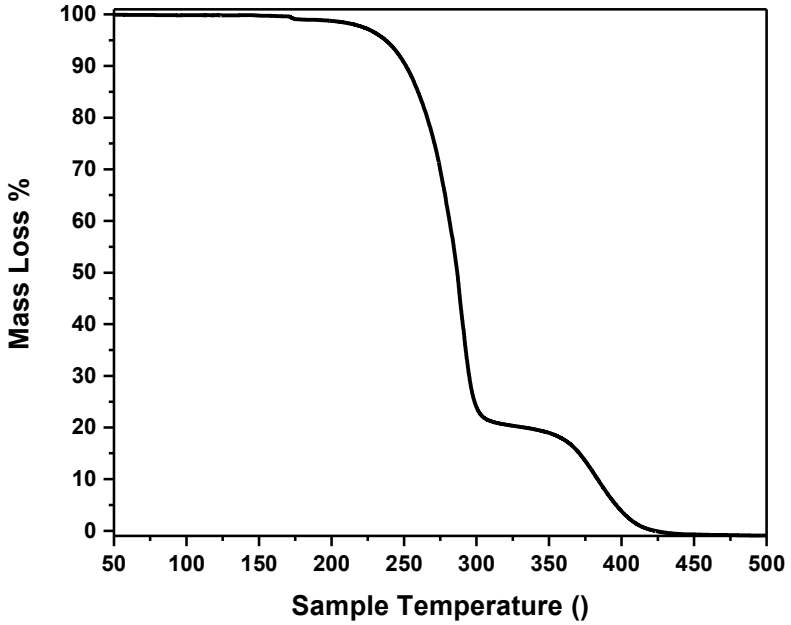

Figure S67. TGA trace for PLLA-PCHO-PLLA copolymer (Table 2, entry 4).

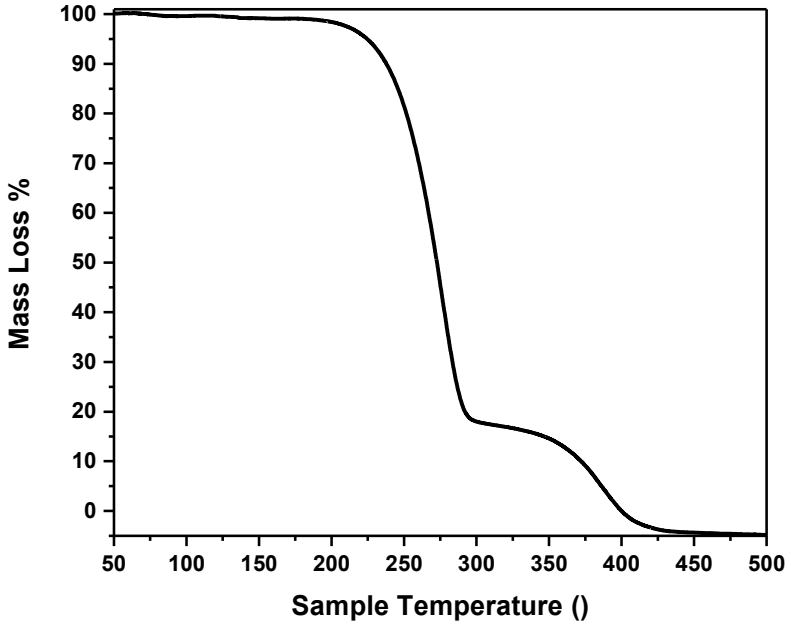

Figure S68. TGA trace for PLLA-PCHO-PLLA copolymer (Table 2, entry 5).

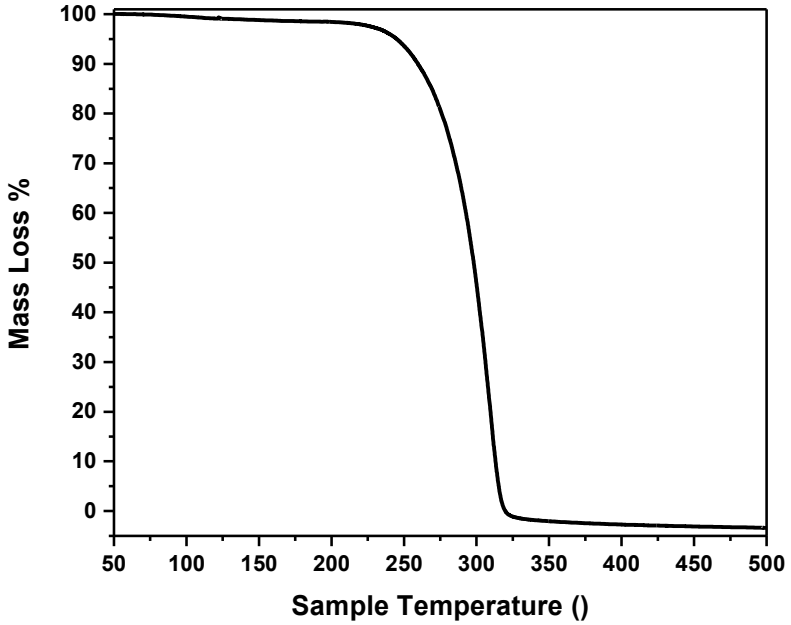

Figure S69. TGA trace for PLLA-PTMC copolymer (Table 2, entry 6).

X-ray data

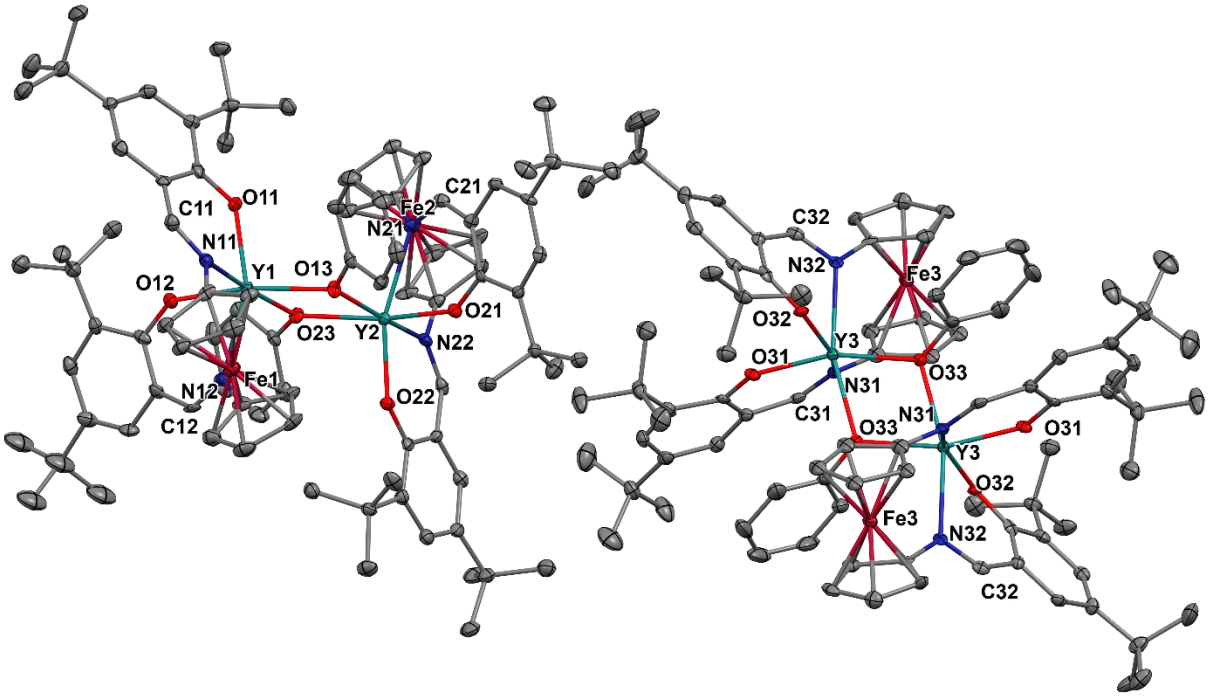

Figure S70. Thermal ellipsoid (50% probability) representation of the crystallographically independent molecules of $[(salfen)Y(OPh)]_2$ in the unit cell (CCDC# 2049815). Hydrogen atoms were omitted for clarity. Single crystals suitable for X-ray crystallography were grown from a hexanes solution. A total of 102675 reflections ($-17 \leq h \leq 17$, $-18 \leq k \leq 18$, $-39 \leq l \leq 39$) were collected at T = 100 K with $2\vartheta_{max} = 50.00°$, of which 23299 were unique. The residual peak and hole electron density were 1.62 and -0.83 eA^{-3}. The least-squares refinement converged normally with residuals of $R_1 = 0.0550$ and GOF = 0.965. Crystal and refinement data for $[(salfen)Y(OPh)]_2$: formula $C_{92}H_{110}Fe_2N_4O_6Y_2$, space group P-1, a = 14.8170(17), b = 15.3498(18), c = 33.240(4) Å; α = 84.575(2), β = 81.112(2), γ = 62.305(2)°; V = 6611.2(13) $Å^3$; Z = 3; λ = 0.71073 Å; μ = 1.678 mm^{-1}; d_{calc} = 1.249 $g \cdot cm^{-3}$; F(000) = 2604, $R1$ = 0.1025 and $wR2$ = 0.1370 (based on all data, I > 2δ*(I)*).